Shugoshin maintains mitotic arrest in response to improper kinetochore-microtubule interactions independent of the Bub1-pH2A axis

Satya Dev Polisetty[1], Krishna Bhat[1], Ivan Clark[2], Kevin Hardwick[2], Kaustuv Sanyal[1*]

[1]Molecular Mycology Laboratory, Molecular Biology and Genetics Unit, Jawaharlal Nehru Centre for Advanced Scientific Research, Bengaluru, India.

[2]Institute of Cell Biology, University of Edinburgh, Edinburgh, United Kingdom.

*Corresponding author

Key Words

Chromosome segregation, kinetochore-microtubule attachments, spindle assembly checkpoint (SAC), checkpoint maintenance, *Cryptococcus neoformans*, spindle pole body (SPB).

Abstract

During chromosome segregation, the spindle assembly checkpoint (SAC) detects errors in kinetochore-microtubule attachments. Timely activation and maintenance of the SAC until defects are corrected is essential for genome stability. Here, we show that *SGO1* codes for shugoshin, a tension-sensing protein, that ensures the maintenance of SAC signals in response to unattached kinetochores during mitosis in a basidiomycete budding yeast *Cryptococcus neoformans*. Sgo1 maintains optimum levels of Aurora B^{Ipl1} kinase and protein phosphatase 1 (PP1) at kinetochores. The absence of Sgo1 results in the loss of Aurora B^{Ipl1} with a concomitant increase in PP1 levels at kinetochores. This leads to a premature reduction in the kinetochore-bound Bub1 levels and early termination of the SAC signals. Surprisingly, the SAC maintenance function of Sgo1 is independent of the Bub1 kinase activity in this budding yeast. Sgo1 is predominantly localized to spindle pole bodies (SPBs) and along the mitotic spindle. In the absence of proper kinetochore-microtubule attachments, Sgo1 reinforces the Aurora B^{Ipl1} kinase- PP1 phosphatase balance, which is critical for maintaining the SAC response.

Introduction

The precise segregation of duplicated chromosomes in mitosis depends on the stable attachment of kinetochores with microtubules (MTs) and proper orientation on the mitotic spindle. The kinetochore is a multi-subunit protein complex composed of inner and outer layers (Musacchio and Desai, 2017). The inner kinetochore assembles onto centromeric chromatin and is constitutively associated with DNA. Subsequently, the outer kinetochore assembles and promotes the attachment of MTs emanating from centrosomes or spindle pole bodies (SPBs). Apart from playing a role in MT attachment, the kinetochore also acts as a signaling platform for recruiting mitotic surveillance components that detect unattached or improperly attached kinetochores (Lara-Gonzalez et al., 2021, Zich and Hardwick, 2010, Musacchio and Salmon, 2007). Once errors are detected, cells remain arrested at metaphase until rectified.

Mitotic surveillance systems monitoring erroneous kinetochore-MT attachments include the spindle assembly checkpoint (SAC) and a chromosome passenger complex (CPC) component, Aurora B^{Ipl1} kinase. The SAC comprises Mad1, Mad2, BubR1, Bub3, and the kinases Bub1 and Mps1 (Lara-Gonzalez et al., 2021). The SAC machinery conveys a 'wait anaphase' signal (MCC, the mitotic checkpoint complex) during cell division in response to unattached kinetochores that inhibits the anaphase-promoting complex (APC/C^{Cdc20}) from ubiquitylating B-type cyclins and securin (Hardwick et al., 2000, Musacchio, 2015, Sudakin et al., 2001). Upon the formation of proper kinetochore-MT attachments, the SAC is silenced. APC/C^{Cdc20} inhibition is relieved, resulting in the degradation of B-type cyclins and securin, thus promoting mitotic exit and sister chromatid separation (Cohen-Fix et al., 1996, King et al., 1996).

Tension across sister-kinetochores attached to MTs is important in ensuring high fidelity of chromosome segregation. Tensionless kinetochore-MT attachments, if not rectified, result in the missegregation of chromosomes. Aurora B^{Ipl1} acts as a tension sensor, detecting tension across sister-kinetochores (Biggins and Murray, 2001, Tanaka et al., 2002, Hauf et al., 2003, Pinsky et al., 2006). In response to tensionless kinetochore-MT attachments, phosphorylation of outer kinetochore by Aurora B^{Ipl1} results in the destabilization of kinetochore-MT interactions, leading to the generation of unattached kinetochores (Cheeseman et al., 2006, Ciferri et al.,

2008) indirectly activating the SAC. Several reports implicate that Aurora B^{Ipl1} can also directly activate the SAC machinery in response to unattached kinetochores, indicating that the function of Aurora B^{Ipl1} is not just limited to detecting tensionless attachments (Kallio et al., 2002, Petersen and Hagan, 2003, Saurin et al., 2011, Santaguida et al., 2011, Pinsky et al., 2009). The kinase activity of Aurora B^{Ipl1} also counteracts PP1 phosphatase recruitment to kinetochores (Liu et al., 2010). The activity of PP1 at kinetochores is required to terminate the SAC signaling and to help cells proceed into anaphase. PP1 dephosphorylates kinetochore substrates and thus promotes the stabilization of kinetochore-MT attachments (Lara-Gonzalez et al., 2021). Premature recruitment of PP1 to kinetochores results in early termination of the SAC signal and leads to chromosome mis-segregation (Roy et al., 2019).

Shugoshin, another tension sensor, also detects tensionless kinetochore-MT attachments and promotes the biorientation of sister kinetochores during mitosis. Unlike Aurora B^{Ipl1}, shugoshin cannot directly destabilize tensionless attachments but acts as an adaptor protein in recruiting Aurora B^{Ipl1}, thus promoting the biorientation of sister kinetochores. Though it plays an important role in the biorientation of chromosomes, several reports indicate that during mitosis, shugoshin is dispensable for the SAC activation (Indjeian et al., 2005, Vanoosthuyse et al., 2007, Sane et al., 2021). Shugoshin primarily localizes to centromeres, and phosphorylation of histone H2A (T120, humans/S121, yeasts) by the SAC component Bub1 kinase plays a central role in targeting it to centromeres (Kawashima et al., 2010, Fernius and Hardwick, 2007).

Mechanisms involved in monitoring kinetochore-MT attachments are not extensively studied in basidiomycete yeasts such as *Cryptococcus neoformans* with a significantly altered kinetochore structure (van Hooff et al., 2017, Sridhar et al., 2021). Studies to explore the roles of SAC components Bub1 (Madbub), Mps1, and Mad1 in the checkpoint response using *C. neoformans* have just begun (Leontiou et al., 2022, Aktar et al., 2023). Here, we probed the role of an evolutionarily conserved protein, shugoshin, in *C. neoformans* in monitoring the kinetochore-MT attachments during mitosis. We propose that shugoshin performs this function by maintaining higher Aurora B^{Ipl1} and lower PP1 levels at kinetochores during MT depolymerizing conditions. Strikingly, we observed that the kinase activity of Bub1 is dispensable for

the shugoshin's checkpoint maintenance function, indicating that the mechanism of shugoshin targeting is rewired during *C. neoformans* mitosis.

Results

Shugoshin is required for efficient metaphase arrest in response to microtubule depolymerizing drugs

SGO1 (FungiDB ORF ID: CNAG_05516) encodes the only form of shugoshin that is expressed in *C. neoformans.* The putative 645-aa-long protein coded by *SGO1* has an N-terminal coiled-coil domain and a C-terminal basic SGO motif (Fig 1A; Supplementary Fig 1A and B). Multiple sequence alignment of amino acid sequences revealed the presence of conserved residues required for PP2A binding (Supplementary Fig 1B) (Xu et al., 2009). The SGO motif in *C. neoformans* shugoshin also possesses a conserved lysine residue (K382) that is required for the binding of shugoshin to phosphorylated histone H2A (Supplementary Fig 1B) (Kawashima et al., 2010, Liu et al., 2013, Fernius and Hardwick, 2007). Previous studies reported that shugoshin plays a role in ensuring proper kinetochore-MT attachments during mitosis (see reviews (Gutierrez-Caballero et al., 2012, Marston, 2015)). Mutants affecting kinetochore-MT interactions and proteins participating in the error correction machinery and SAC, are hypersensitive to MT depolymerizing drugs. To test if Sgo1 contributes to the fidelity of mitotic chromosome segregation, we created *sgo1* null mutants in *C. neoformans.* While Sgo1 was found to be dispensable for growth, *sgo1* null mutant cells displayed sensitivity to a MT-depolymerizing drug, thiabendazole (TBZ), similar to that of SAC mutant *mad2* (Fig 1B). These results suggest that *sgo1Δ* mutant cells in the basidiomycete yeast *C. neoformans* have phenotypes similar to those of ascomycete yeasts such as *Saccharomyces cerevisiae*, *Schizosaccharomyces pombe* and *Candida albicans* (Indjeian et al., 2005, Kitajima et al., 2004, Sane et al., 2021).

Next, we sought to test if enhanced sensitivity to the MT poison observed in *sgo1Δ* mutant cells accentuate when combined with *mad2Δ* mutant. To test this, we created *sgo1Δ mad2Δ* double mutants. Such double mutant cells exhibited synthetic lethality in the presence of TBZ (Fig 1B), indicating that both Sgo1 and Mad2 are required for an efficient SAC response in MT-depolymerizing conditions. If shugoshin is required for an efficient SAC response in *C. neoformans*, it is expected that the *sgo1Δ*

mutant, when combined with a kinetochore mutant, would enhance sensitivities to TBZ. To explore this possibility, we used null mutant cells of a recently reported basidiomycete-specific kinetochore linker protein bridgin (Bgi1). It has been shown that *bgi1Δ* mutants are viable but exhibit gross chromosomal missegregation (Sridhar et al., 2021). *bgi1Δ* mutants, combined with *mad2Δ*, displayed enhanced sensitivity to TBZ compared to each of the single mutants alone (Sridhar et al., 2021). The spotting assay indicated that *sgo1Δ bgi1Δ* double mutant cells are hypersensitive to TBZ, similar to that of *mad2Δ bgi1Δ* (Supplementary Fig 2). Together, these results reveal that shugoshin plays a role in proper kinetochore-MT interactions and/or monitors defective attachments in response to spindle poison.

MT-depolymerizing drugs arrest wild-type cells at metaphase in the large-budded stage with an undivided nucleus. Only when the defects are rectified will such cells proceed to complete the cell division. To verify whether *sgo1Δ* mutants can induce metaphase arrest when MTs are depolymerized, we performed a microscopy-based assay to score for the cell cycle defects associated with *sgo1Δ* mutants by treating cells with nocodazole (Fig 1C). Nocodazole-treated wild-type cells of *C. neoformans* arrest at the large-budded stage with a visibly condensed chromatin mass (Fig 1D). After 240 min of nocodazole treatment, >90% of wild-type cells were at the large-budded stage with a condensed undivided nucleus (Fig 1D and Supplementary Fig 1C, D, and E). As expected, the checkpoint defective mutant (*mad2Δ*) failed to arrest cells at the large-budded stage (Fig 1D). In the *sgo1Δ* mutants, though we initially observed an increase in the proportion of large-budded cells compared to *mad2Δ* mutants, after 240 min post-nocodazole treatment, the large-budded cell population significantly reduced (Fig 1D). Moreover, unlike wild-type, most large-budded cells in *sgo1Δ* mutants had an uncondensed chromatin mass similar to *mad2Δ* mutant cells (Supplementary Fig 1C, D, and E). In the case of *sgo1Δ mad2Δ* double mutants, no significant differences in the proportion of large-budded cells were observed when compared to *sgo1Δ* and *mad2Δ* single mutants (Fig 1D). Estimating the ploidy content in nocodazole-treated cells using flow cytometry (Fig 1E) revealed that wild-type cells arrested at 2n ploidy level. On the other hand, *mad2Δ* cells shifted towards 4n, indicating a failure in arresting cells at metaphase and initiating the next cell cycle events. Unlike *mad2Δ, sgo1Δ* cells displayed a ploidy content of 2n and 4n, revealing the presence of cells that are delayed at metaphase and cells that have

initiated the next round of DNA replication. Similar results were also obtained in *sgo1Δ mad2Δ* double mutants. Taken together, we show that shugoshin is required for an efficient metaphase arrest in response to unattached kinetochores induced by MT-depolymerizing drugs.

***sgo1Δ* mutant cells fail to maintain the SAC component Bub1 at kinetochores in response to prolonged microtubule depolymerization**

Why are *sgo1Δ* mutant cells not arrested when treated with a MT poison at metaphase? It is possible that *sgo1Δ* mutant cells arrest at metaphase immediately after being treated with the MT poison but were unable to maintain the arrest upon prolonged exposure to the drug. To test this, we localized the SAC component Bub1 (Fig 2A) tagged with GFP in wild-type and *sgo1Δ* cells. A recent report (Leontiou et al., 2022) suggested that Bub1 localizes to kinetochores in *C. neoformans* and plays a role in SAC-mediated arrest. We synchronized *C. neoformans* cells by arresting them at G2 using hypoxia (Ohkusu et al., 2004) and released them in the presence of nocodazole (refer to Materials and Methods for further details) (Fig 2B). Inducing physical hypoxia in *C. neoformans* results in 'unbudded' G2 arrest. These G2-arrested cells enter mitosis synchronously when subjected to extensive aeration. Upon release into nocodazole-containing media, wild-type cells accumulated at the large-budded stage with GFP-Bub1 signals, which were maintained until the end of the experiment (Fig 2C and D). In case of *sgo1Δ* cells, the proportion of Bub1-positive large-budded cells increased similarly to that of wild-type until 120 min. However, beyond 200 min post-nocodazole treatment, a sudden decline in the proportion of Bub1-positive large-budded cells was observed in the mutant (Fig 2C and D). Studies in *S. pombe* have shown that the kinase-dead version of Bub1 is checkpoint-proficient but fails to maintain prolonged SAC arrest (Fernius and Hardwick, 2007)**.** A similar observation was reported in *C. neoformans*, where *bub1-kd* mutant cells failed to sustain the arrest induced by nocodazole (Leontiou et al., 2022)**.** To understand how checkpoint responses differ in *sgo1Δ* from *bub1-kd,* we compared GFP-Bub1 localization dynamics in hypoxia-synchronized cells treated with nocodazole (Fig 2D). Though neither *sgo1Δ* nor *bub1-kd* mutant cells could maintain the arrest like the wild-type, *bub1-kd* cells were able to maintain the arrest longer than *sgo1Δ* cells.

Moreover, Bub1 signal intensities in *sgo1Δ* mutants were significantly reduced compared to the wild-type (Fig 2E). To further support these observations, we resorted to a single-cell microfluidics assay to quantitatively measure the checkpoint response in individual cells treated with the MT poison (Fig 2F and G). Using this system, we probed the GFP-Bub1 dynamics in wild-type, *sgo1Δ*, *bub1-kd,* and *mad1Δ* mutant cells treated with nocodazole. Similar to the results observed in the experiment performed with the synchronized cells, neither *sgo1Δ* nor *bub1-kd* mutant cells could maintain checkpoint arrest like wild-type as indicated by the lower mean kinetochore residence times of Bub1 (Fig 2G). Checkpoint defective *mad1Δ* mutant cells were used as a control. These results reveal that *sgo1Δ* cells, similar to *bub1-kd* cells, are proficient in checkpoint activation and cannot maintain checkpoint signals during prolonged treatment with nocodazole.

Aurora B^{Ipl1} maintenance at kinetochores is affected in *sgo1Δ* mutants during prolonged checkpoint arrest

Shugoshin interacts with CPC proteins and helps in either the recruitment or maintenance of CPC components at centromeres/kinetochores in *S. cerevisiae*, *S. pombe* and humans (Hindriksen et al., 2017, Marston, 2015). Previously, we established the role of Aurora B^{Ipl1} (a CPC component) in regulating nuclear division during mitosis in *C. neoformans* (Varshney et al., 2019). Although it has been shown that the entry of Aurora B^{Ipl1} into the nucleus coincides with the nuclear envelope breakdown (NEBD), its localization to kinetochores remained unexplored. In this study, we colocalized Aurora B^{Ipl1} with the inner kinetochore protein CENP-A at different cell cycle stages (Supplementary Fig 3A). During G2, when kinetochores are clustered, we could only detect weak signals of Aurora B^{Ipl1} that intensified as cells entered metaphase. Apart from the kinetochore localization, we could also observe spindle-like localization of Aurora B^{Ipl1} during anaphase (Supplementary Fig 3A). Upon treatment with nocodazole, we observed colocalization of Aurora B^{Ipl1} with kinetochores (Supplementary Fig 3B). To test whether kinetochore localization of Aurora B^{Ipl1} is affected in *sgo1Δ* cells in *C. neoformans*, we synchronized both wild-type and *sgo1Δ* mutant cells by inducing physical hypoxia followed by a release in nocodazole-containing media (Fig 2B). We scored for Aurora B^{Ipl1}-3xGFP-positive large-budded cells. In *sgo1Δ,* we observed a reduced proportion of Aurora B^{Ipl1}-positive large-budded cells over time compared to wild-type(Fig 3A and B). Similar to

the Bub1 levels in *sgo1Δ* mutant cells, a reduction in the intensity of the Aurora B^{Ipl1} signals in the *sgo1Δ* cells was also observed compared to the wild-type (Fig 3C). Taken together, we conclude that Sgo1 is required to maintain Bub1 and Aurora B^{Ipl1} at kinetochores when MTs are depolymerized.

Aurora B^{Ipl1} is required for the maintenance of Bub1 at kinetochores in response to microtubule depolymerization

Reduced Aurora B^{Ipl1} levels at kinetochores in *sgo1Δ* cells prompted us to test whether the absence of Aurora B^{Ipl1} leads to failure of checkpoint arrest when treated with MT depolymerizing agents. For conditional depletion of Aurora B^{Ipl1}, we placed the gene under the *GAL7* promoter. We treated Aurora B^{Ipl1}-overexpressed (permissive, galactose media) and Aurora B^{Ipl1}-depleted (non-permissive, glucose media) cells with nocodazole (Fig 3D). We assayed for large-budded cells with a condensed chromatin mass as observed at metaphase. Cells overexpressing Aurora B^{Ipl1} and treated with nocodazole displayed a higher proportion of large bud arrested cells. In contrast, cells depleted of Aurora B^{Ipl1} failed to arrest at the large-budded stage and exhibited an increase in the proportion of tri-budded cells (Supplementary Fig 4A and B). Moreover, approximately 50% of the large-budded cells displayed an uncondensed nuclear mass, similar to what was observed in *mad2Δ* mutants (Supplementary Fig 4A and B). These results suggest that Aurora B^{Ipl1} is required for an efficient metaphase arrest when cells are treated with a spindle poison in *C. neoformans*.

To confirm these observations further, we examined GFP-Bub1 localization dynamics in cells depleted of Aurora B^{Ipl1} and treated with nocodazole (Fig 3E). Aurora B^{Ipl1}-depleted cells subjected to nocodazole treatment for 120 and 240 min were able to load Bub1 initially but failed to maintain Bub1 at kinetochores upon prolonged treatment with nocodazole (Fig 3E and F), similar to what was observed in *sgo1Δ* mutant cells. We also noticed a significant reduction in the levels of Bub1 at kinetochores in Aurora B^{Ipl1}-depleted cells similar to that of *sgo1Δ* mutants (Fig 3G). These results reveal that Aurora B^{Ipl1} in *C. neoformans* helps maintain Bub1 at kinetochores in the presence of nocodazole.

Shugoshin antagonizes the recruitment of PP1 at kinetochores in response to nocodazole treatment

The kinase activity of Aurora B^{Ipl1} and the phosphatase activity of PP1 are antagonistic at kinetochores (Tatchell et al., 2011, Lesage et al., 2011). We hypothesized that a reduction in Aurora B^{Ipl1} levels leads to increased PP1 levels (Fig 4A), and higher PP1 levels may lead to the loss of Bub1 from kinetochores. We expressed PP1-GFP (FungiDB ORF ID CNAG_03706; Supplementary Fig 5) in a CENP-A-mCherry expressing strain (CNKB003). First, we studied the effect of *sgo1Δ* on PP1 localization during nocodazole treatment (Fig 4B). Both wild-type and *sgo1Δ* cells exhibited GFP-PP1 signals at kinetochores during the metaphase-arrested stage. Quantifying the fluorescence signal intensity of PP1 revealed a marginal but significant increase in the GFP-PP1 signal intensities at kinetochores in *sgo1Δ* compared to wild-type cells (Fig 4C). A similar result was observed when Aurora B^{Ipl1}-depleted cells were treated with nocodazole (Fig 4D and E). The SAC can be silenced by dephosphorylation of MELT repeats on $Knl1^{Spc105}$ with the help of PP1. As a result, checkpoint components are removed from kinetochores (Pinsky et al., 2009, Rosenberg et al., 2011, Meadows et al., 2011, Espeut et al., 2012, Vanoosthuyse and Hardwick, 2009, Nijenhuis et al., 2014). Premature recruitment of PP1 to kinetochores is detrimental and leads to chromosome mis-segregation (Roy et al., 2019). Based on the results described above, we propose that the increase in PP1 levels at kinetochores leads to the loss of Bub1 signals in the absence of shugoshin or Aurora B^{Ipl1}, which interferes with the SAC maintenance in MT depolymerizing conditions.

The kinase activity of Bub1 is dispensable for the function of shugoshin during mitosis in *C. neoformans*

Thus far, we reveal an unknown role of Sgo1 in maintaining Bub1 through the balance of Aurora B^{Ipl1} and PP1 at kinetochores in *C. neoformans* (Fig 5A). Studies from several yeast species and humans reveal that Bub1 is one of the major factors that recruits shugoshin to centromeres (Fig 5A) (Kawashima et al., 2010, Liu et al., 2013). To study if the Bub1 kinase activity required for shugoshin's function is evolutionarily conserved in *C. neoformans*, we utilized the kinase-dead (*bub1-kd*) mutant of Bub1. *In vitro* assays reported earlier (Leontiou et al., 2022) revealed that Bub1 could phosphorylate the reconstituted human H2A containing nucleosomes, and kinase-dead mutants of Bub1 fail to phosphorylate. We performed a genetic interaction assay by scoring the TBZ sensitivity of *sgo1Δ*, *bub1-kd*, and *sgo1Δ bub1-*

kd mutants (Fig 5B). If both Sgo1 and Bub1 kinase activity function in the same pathway in *C. neoformans*, one would expect little to no change in the sensitivity of double mutants compared to either of the single mutants, ***sgo1Δ*** and *bub1-kd*. By dilution spotting assay, we observed that the *bub1-kd* ***sgo1Δ*** double mutant cells behaved like that of the ***sgo1Δ*** mutant (Fig 5B). Moreover, the sensitivity of ***sgo1Δ*** mutant cells to TBZ is higher than that of *bub1-kd* mutant. These results hint that the kinase activity of Bub1 is dispensable for shugoshin's checkpoint function during mitosis in *C. neoformans*.

The lysine residue K382 of Sgo1 in *C. neoformans* corresponds to lysine K492 in Sgo1 of humans (Supplementary Fig 1B). This residue is known to play a role in binding to phosphorylated H2A (Kawashima et al., 2010, Liu et al., 2013). A mutation in the lysine residue of shugoshin in fission yeast (K298) and humans (K492) results in the loss of centromeric localization of shugoshin in mitosis. To test the role of the evolutionarily conserved lysine residue in *C. neoformans*, we mutated K382 to alanine. The plasmid constructs harboring either wild-type *SGO1* or a *sgo1-K382A* allele were integrated into the *SAFE HAVEN* locus of the ***sgo1Δ*** strain (Fig 5C, *top panel*). If the kinase activity of Bub1 is indeed dispensable for shugoshin's checkpoint function during mitosis, the strain carrying *sgo1-K382A* allele would rescue the sensitivity to spindle poisons. Spotting assays on TBZ plates revealed that *sgo1-K382A* mutants behaved like that of wild-type cells (Fig 5C, *bottom panel*). These results confirm that the kinase activity of Bub1 is dispensable for the SAC function of shugoshin in *C. neoformans.*

Shugoshin is enriched at the spindle pole bodies (SPBs) and localizes to the spindle during mitosis

Having established that Bub1 kinase activity is not required for the SAC maintenance function of Sgo1, we examined the cell cycle localization dynamics of Sgo1 in *C. neoformans*. Shugoshin localizes to the kinetochore during cell division in most species studied (Marston, 2015) (Supplementary Fig S7, *right*). To find the sub-cellular localization of Sgo1, we expressed GFP-Sgo1 from its native locus in the CENP-A-mCherry tagged strain. We synchronized the cells using hypoxia to examine the cell cycle stage-specific localization of Sgo1. No signals of Sgo1 could be observed during most of the interphase. In G2, where all centromeres cluster as a

single punctum (Kozubowski et al., 2013, Sridhar et al., 2021), we observed Sgo1 signals near clustered centromeres (Fig 6A). Upon entry into mitosis, Sgo1 appeared as two distinct puncta that flanked the bar-like signals of CENP-A. Apart from the punctate signals of Sgo1, we observed weak signals along the pole-to-pole axis during metaphase and anaphase that resembled spindle-like localization. To examine whether Sgo1 localizes to spindle pole bodies (SPBs), we expressed Tub4-mCherry (γ-tubulin) in the GFP-Sgo1 expressing strain. GFP-Sgo1 signals colocalized with SPBs during G2 and mitotic stages (Fig 6B), indicating that Sgo1 localizes predominantly to SPBs during the mitosis in *C. neoformans*.

To test if the spindle-like localization during mitosis depends on the spindle MT integrity, we arrested cells at metaphase using two methods. First, we used nocodazole to depolymerize MTs that activate the SAC and arrest cells at metaphase. Second, we depleted Cdc20, an anaphase-promoting complex/cyclosome (APC/C) component. Depletion or inactivation of Cdc20 leads to metaphase arrest in *S. cerevisiae* (Hwang et al., 1998). Upon treating *C. neoformans* cells with nocodazole, we observed that Sgo1 colocalized with the SPB (Fig 6C). On the other hand, depletion of Cdc20 by placing it under the galactose regulatable promoter (*GAL7*) resulted in metaphase arrest, and the spindle-like localization of shugoshin along the pole-to-pole axis was maintained (Fig 6D). These observations led us to conclude that the spindle-like localization of Sgo1 requires intact MTs during mitosis.

The tension-sensing function of shugoshin is conserved in *C. neoformans*

Shugoshin senses tensionless attachments by recruiting several factors that play a role in correcting tensionless attachments (Marston, 2015). Cohesin is a molecular glue that holds two sister chromatids together during mitosis until metaphase. Cohesin plays an essential role in generating tension that resists the pulling force of MTs aiding high-fidelity chromosome segregation (Guacci et al., 1997, Michaelis et al., 1997). Loss of cohesion at centromeres results in tensionless kinetochore-MT attachments. To test if Sgo1 in *C. neoformans* can detect tensionless attachments, we depleted one of the cohesin subunits, Scc1/Mcd1/Rad21, by placing it under the *GAL7* promoter both in the wild-type and ***sgo1Δ*** mutant cells. *C. neoformans* Scc1 (FungiDB ORF ID CNAG_01023) harbors N- and C-terminal Scc1 domains

(Supplementary Fig 6A and B). We show that, like *S. cerevisiae* and *S. pombe, SCC1* in *C. neoformans* is essential for viability (Supplementary Fig 6C). Upon depletion of Scc1, a high proportion of wild-type cells are arrested at the large-budded stage (Supplementary Fig 6D, E, and F). In contrast, the ***sgo1Δ*** mutants depleted of Scc1 did not show such an increase in the proportion of large-budded cells, indicating that shugoshin plays a role in detecting tensionless kinetochore-MT attachments and delays the cell cycle progression.

Discussion

In this study, we characterized the mitotic functions of shugoshin in *C. neoformans*. The only form of shugoshin, coded by *SGO1*, localizes to SPBs and along the mitotic spindle during mitosis in *C. neoformans* rather than at centromeres/kinetochores. In response to prolonged MT depolymerization, Sgo1 maintains adequate Aurora B^{Ipl1} levels at kinetochores to antagonize premature phosphatase action of PP1 at kinetochores. Thus, by regulating an optimum balance of the protein kinase Aurora B^{Ipl1} and the protein phosphatase PP1, shugoshin retains checkpoint responses until errors are corrected. Together, we discovered a previously unknown role of Sgo1 in regulating PP1 at kinetochores. We also demonstrated that the checkpoint maintenance function of Sgo1 is independent of the evolutionarily conserved Bub1 kinase activity-mediated targeting of Sgo1 to centromeres/kinetochores.

Sgo1 is not required to activate the SAC; rather, it helps prolong the SAC response by maintaining the levels of Bub1 at kinetochores in *C. neoformans*. A similar result was also observed in the absence of Aurora B^{Ipl1} in response to MT depolymerization conditions. Studies in *S. cerevisiae*, *S. pombe*, flies, and humans reveal that shugoshin interacts with the chromosome passenger complex (CPC) and is required for either recruitment or maintenance of Aurora B^{Ipl1} to correct tensionless kinetochore attachments in an organism-specific manner (Hindriksen et al., 2017, Marston, 2015). We show that apart from maintaining Bub1 levels at kinetochores, Sgo1 is also required to maintain Aurora B^{Ipl1} levels when treated with nocodazole. In response to MT depolymerization, ***sgo1Δ*** mutants fail to maintain Aurora B^{Ipl1} and Bub1 levels at kinetochores. Even Aurora B^{Ipl1}-depleted cells were unable to maintain Bub1 at kinetochores. At this point, we hypothesize that Sgo1 regulates the SAC function through Aurora B^{Ipl1} in one of the two possible ways: a) by maintaining high Aurora B^{Ipl1} activity at kinetochores, thereby preventing the action of PP1 in

terminating SAC signals, or b) by regulating activities of Mps1 and Bub1 (Saurin et al., 2011, Roy et al., 2022) at kinetochores, thereby modulating the SAC response. The fact that we observe an increase in the levels of PP1 at kinetochores in the reduced levels of Aurora B^{Ipl1} indicates that Sgo1, more likely, acts through Aurora B^{Ipl1} to antagonize the activity of PP1 at kinetochores thereby preventing premature SAC termination.

Bub1 plays a major role in targeting shugoshin to kinetochores in *S. cerevisiae* and *S. pombe*, *Xenopus laevis,* and humans (Liu et al., 2013, Kawashima et al., 2010, Boyarchuk et al., 2007) (Fig 5A). Intriguingly, the checkpoint maintenance function of Sgo1 is not mediated through Bub1 kinase activity during mitosis in *C. neoformans*. Moreover, Sgo1 in *C. neoformans* shows non-canonical localization at SPBs and along the mitotic spindle instead of being at centromeres/kinetochores. The reason that the kinase activity of Bub1 is dispensable for shugoshin's function during mitosis could be due to the unusual localization of shugoshin. The centromeric localization of Drosophila MEI-S332 (shugoshin) during meiosis is antagonized by the kinase activity of polo-like kinase (Plk1/Cdc5) (Clarke et al., 2005). In humans, Plk1-mediated phosphorylation of shugoshin targets a splice variant of Sgo1 to centrosomes during interphase (Wang et al., 2008). Even though the lysine residue (K382) required for the kinetochore targeting is evolutionarily conserved in *C. neoformans* Sgo1, it will be worth testing if the action of Plk1/Cdc5 prevents the association of Sgo1 to kinetochores, especially in mitosis and thereby targeting it to SPBs.

The fact that Sgo1 is not required for the SAC activation but for the maintenance of the SAC response via maintaining a balance between Aurora B^{Ipl1}-PP1 at kinetochores also explains why ***sgo1Δ mad2Δ*** double mutants are synthetic lethal in the presence of MT depolymerizing drugs. The observed synergy indicates that both Sgo1 and Mad2 act in different pathways, where Sgo1 may play a role in the biorientation of chromosomes that functions via the Aurora B^{Ipl1}-PP1-Bub1 axis.

How does shugoshin play a role in checkpoint maintenance and tension sensing while localizing to spindle MTs and SPBs but not at kinetochores? We speculate that in MT depolymerizing conditions, SPBs are not separated, and kinetochores/centromeres lie near SPBs (Supplementary Fig 7, *left*) (Funabiki et al.,

1993). This proximal association of kinetochores to SPBs brings unattached kinetochores close to shugoshin present on the SPBs (Fig 6E). The SPB-associated Sgo1 may utilize this mechanism and position near the Aurora B^{Ipl1} gradient on kinetochores, thereby influencing the Aurora B^{Ipl1} localization or its maintenance at kinetochores. In response to the above situations, Sgo1 promotes lower levels of PP1 through Aurora B^{Ipl1}, thus influencing the SAC maintenance (Fig 6E). Once errors are corrected and sister-kinetochores are bioriented, the spatial proximity of Sgo1 to Aurora B^{Ipl1} gradient at kinetochores is reduced, leading to a shift towards reduced Aurora $B^{Ipl1}$and increased PP1 activity/levels at kinetochores resulting in the termination of SAC signaling.

Altogether, this study illustrates the functional diversity of an evolutionarily conserved protein, shugoshin. A spatio-temporal balance of kinase and phosphatase activity is crucial for proper kinetochore-MT attachments and SAC signaling. Sgo1 monitors the kinetochore-MT attachment state in mitosis by balancing Aurora B^{Ipl1} and PP1 levels at kinetochores. The SAC maintenance function of Sgo1 depends neither on the kinase activity of Bub1 nor the centromeric localization Sgo1. It is tempting to speculate that the SAC maintenance is mediated via direct or indirect binding of Sgo1 to SPBs and along the spindle MTs. Further investigation is needed to confirm this hypothesis.

Materials and Methods

Strains and media growth conditions

C. neoformans cultures were grown and maintained on YPD (1% yeast extract, 2% peptone, and 2% dextrose) and YPG (1% yeast extract, 2% peptone, and 2% galactose) media at 30°C unless specified. YPD+1M sorbitol or YPG+1M sorbitol plates were used for transformation. For the selection of transformants, 100 µg/mL of nourseothricin (NAT, clonNAT, Werner BioAgents), 180 µg/mL neomycin (G-418, Sigma-Aldrich), and 220 µg/mL of hygromycin (HiMedia) were used.

Biolistic transformation

The biolistic transformation was done based on a previously described method (Davidson et al., 2000). Approximately 5 mL of *C. neoformans* culture was grown overnight, centrifuged at 4,000 rpm for 5 min, and resuspended in 300 µL sterile

dH_2O. Around 300 µL of cell suspension was spread on the YPD+1M sorbitol plate and dried. Gold micro-carrier beads (0.6 µm) coated with 2-5 µg of DNA were prepared, and 10 µL of 2.5 M $CaCl_2$, 2 µL of 1M spermidine free base (Sigma-Aldrich) were added. The mixture was vortexed for 30 s, incubated for 10 min at room temperature, centrifuged, washed with 500 µL of 100% ethanol, and resuspended in 10 µL of 100% ethanol. The solution was placed on a micro-carrier disk and allowed to dry. Dried disks were placed in the biolistic transformation apparatus (Biolistic® PDS-1000/He Particle Delivery System). Helium gas pressure of approximately 1300 psi under a vacuum of a minimum of 25 inches of Hg was generated to bombard the cells with micro-carrier beads. The cells were incubated for 5-6 h in YPD+1M sorbitol medium at 30°C. Cells were then plated on YPD+NAT/NEO/HYG selection plate and incubated at 30°C for 3-4 days.

Strains and plasmids

Lists of strains, plasmids, and primers used in this study are provided in Tables S1-S3. The construction of *C. neoformans* strains and plasmids is detailed below.

***GFP-SGO1* strains**

The fluorescent fusion protein of shugoshin was generated by cloning the 1200 bp homology region and the *SGO1* promoter into the pVY7 plasmid containing the GFP and NAT sequences. GFP was tagged to the N-terminal region of the *SGO1* gene. The primers used for generating the clone are listed in Table S3. The 1200 bp homology region and a 500 bp *SGO1* promoter region were amplified from the *SGO1* gene using *C. neoformans* (H99) genomic DNA. The individual PCR fragments were gel purified. The amplified regions were cloned using BamHI, SacI, and NcoI sites. The final clone was linearized using HindIII and transformed into H99 and CNVY101. The transformants obtained were confirmed by PCR.

***sgo1Δ* strains**

An overlap PCR strategy was used to delete *SGO1* gene in the desired strains. Around 1000 bp region upstream to the start codon (ATG) and 1000 bp downstream region of the stop codon of the *SGO1* ORF was amplified using *C. neoformans* (H99) genomic DNA. The *NEO* resistance marker fragment was amplified from the pLK25 plasmid (Table S2). The individual PCR fragments were gel purified. Using these

individual PCR amplified fragments, a final overlap cassette of ~3800 bp was constructed using primers (Table S3). The final cassette was used to transform *C. neoformans*. The transformants obtained were confirmed by PCR. To delete the *SGO1* gene in different strain backgrounds, the *NEO* marker was swapped with either *NAT* or *HygB* genes amplified from the pVY7 and pSH7G plasmids (Table S2) using the same set of primers. The ***sgo1Δ*** cassette was used to transform H99, CNVY108, SHR741, SHR830, IL102, IL143, CNKB003 and CNSD190 strains. The transformants obtained were screened by PCR.

***TUB4-mCherry* strain**

An overlap PCR strategy was used to tag Tub4 with mCherry at C-terminus. Primers used for overlap cassette construction are listed in Table S3. Around 1000 bp region upstream to the stop codon (without including the stop codon) and 1000 bp 3' UTR region after the stop codon was amplified from the *TUB4* ORF using *C. neoformans* (H99) genomic DNA. The mCherry sequence with antibiotic resistance marker NEO was amplified from the pLK25 plasmid (Table S2). The individual PCR fragments were gel purified. A final overlap cassette of ~4500 bp was constructed using individual PCR fragments. The final cassette was transformed into CNSD127 strain. The transformants obtained were confirmed by PCR.

***GAL7-3xFLAG* tagged *SCC1*, *AURORA B^{IPL1}*, *CDC20* strains**

To place the desired gene under regulatable *GAL7p* along with an N-terminal 3XFLAG sequence, an overlap PCR strategy was used. Around 1000 bp regions upstream (US) and downstream (DS) of the start codon (ATG) of the ORFs of interest were amplified using *C. neoformans* (H99) genomic DNA. *GAL7* promoter with *HygB* resistance gene was amplified from pSH7G plasmid, and the 3xFLAG sequence was introduced using a primer (Table S3). The individual PCR fragments were gel purified. A final overlap cassette was assembled using the individual purified fragments. The cassettes generated were transformed into *C. neoformans* and the positive transformants were confirmed by PCR. The 3xFLAG tagged conditional mutants of *SCC1*, *AURORA B^{IPL1}*, and *CDC20* generated using the strategy mentioned above are listed in Table S1.

AURORA B^{IPL1}-3xGFP mCherry-CENP-A **strain**

The H99 strain expressing Aur B^{Ipl1}-3xGFP and mCherry-CENP-A was generated by the random integration of the plasmid pLKB71 (Table S2). The mCherry-CENP-A construct is expressed using the *H3* promoter. To create the strain, the plasmid backbone of pLKB71 was digested with HindIII and transformed into CNNV113, and the transformants were selected on the YPD-agar plate containing hygromycin selection. The colonies obtained were screened using a Zeiss Axio Observer 7 widefield microscope for the transformants positive for the mCherry-CENP-A signal.

GFP-PP1 mCherry-CENP-A **strain**

The N-terminal GFP fusion protein of PP1 was generated by cloning around 1000 bp homology region and PP1 promoter into the pVY7 plasmid containing GFP and NAT sequences. Around 955 bp PP1 promoter region and 1000 bp PP1 homology region was amplified from PP1 ORF using *C. neoformans* (H99) genomic DNA. The PCR amplicons were gel purified. The digested amplicons of promoter and homology region were cloned into pVY7 using SacI; NcoI and SpeI sites respectively. The final clone was linearized using BglII and transformed into CNVY101 strain, and the positive transformants were confirmed by PCR.

GFP-sgo1-K382A-SH1 **and** ***GFP-SGO1-SH1*** **strains**

The N-terminal GFP fusion protein of wild-type and mutant (K382A) allele of *SGO1* was generated by cloning *SGO1* promoter, *SGO1* ORF, and 3'UTR into the pSD29 plasmid (Table S2) containing the GFP, HygB and *SAFE HAVEN* sequences. Around 2340 bp of *SGO1* ORF and 315 bp of *SGO1* promoter, and 436 bp of 3'UTR were amplified from the *SGO1* gene using *C. neoformans* (H99) genomic DNA. The K382A mutation in the *SGO1* ORF was introduced using overlap PCR. The primers used are listed in Table S3. The individual PCR fragments were gel purified. The purified fragments of *SGO1* promoter, *SGO1* ORF, and 3'UTR were cloned sequentially using SpeI, BamHI, HpaI, NheI, and ApaI sites. The final clone was linearized using XcmI and transformed into CNSD113. The transformants obtained were confirmed by PCR.

Thiabendazole sensitivity assay

For assaying sensitivity to thiabendazole, the $O.D_{600}$ values of overnight cultures of wild-type and mutants used in this study were estimated, and serial dilutions starting from 10^5 cells to 10^1 cells were spotted on YPD-agar, DMF (Dimethyl Formamide); control, and YPD-agar plates with different concentrations of thiabendazole (2.0, 2.5, 3.0 and 4.0 µg/mL). The plates were incubated at 30°C for 24 to 48 h and imaged using a Bio-Rad chemidoc imaging system.

Synchronization of *C. neoformans* by inducing physical hypoxia

For the synchronization of *C. neoformans* cells, we have used a protocol developed by Ohkusu et al., (Ohkusu et al., 2004) which utilizes a two-step protocol for the synchronization. *C. neoformans* cells, when grown in hypoxia conditions, result in unbudded G2 arrest, and cells release synchronously once shifted to extensive aeration conditions. Hypoxia synchrony is a two-step process. First, cells were grown at moderate aeration to 4.0 $O.D_{600}$/mL in a 250 mL flask (Borosil Erlenmeyer flask with a screw cap was used for this experiment) with 50 mL of 1% YPD at 100 rpm, 30 °C. In the second step, the culture was diluted 1.5 times with fresh 1% YPD (final volume of 125 mL) and then incubated further for 5 h. The second step induces physical hypoxia, and at the end of the incubation, most cells get arrested at the unbudded G2 stage.

For the synchronization experiments, we used an overnight culture grown in 1% YPD to inoculate the secondary culture at 0.1 $O.D_{600}$/mL in 1% YPD and grown to 1 $O.D_{600}$/mL at 180 rpm, 30°C. This log phase culture was used for hypoxia synchrony, as mentioned above. The percentage of cells in the unbudded G2 stage was confirmed using a microscope. The culture was diluted to 1 $O.D_{600}$/mL using fresh media, transferred to a sterile falcon or conical flask with appropriate culture volumes, and released under extensive aeration conditions (180 rpm, 30°C).

GFP-Bub1 and Aurora B^{Ipl1}-3xGFP retention assay

To study the localization dynamics of GFP-Bub1 and Aur B^{Ipl1}-3xGFP in response to nocodazole treatment, wild-type and *sgo1Δ* mutants were subjected to hypoxia synchrony, and the cells were released into 1% YPD media containing 1 µg/mL nocodazole. Time points were collected every 40 minutes until 280 min. The cells collected were imaged using a Zeiss Axio Observer 7 widefield microscope.

Imaging GFP-Sgo1 localization in *mCherry-CENP-A* and *TUB4-mCherry* strains

For imaging GFP-Sgo1 colocalization with CENP-A- and Tub4-mCherry tagged proteins, we synchronized cells using physical hypoxia. Cells were released into 1% YPD and collected every 10 min starting from 30 to 90 min. Cells were imaged using a Zeiss Axio Observer 7 widefield microscope.

Budding index calculation

The proportion of unbudded, small-budded, and large-budded cells was calculated based on the budding index (diameter of daughter cell/diameter of mother cell). The diameters of both mother and daughter cells were calculated along the mother-daughter axis using the line tool in Fiji (Schindelin et al., 2012).

Fluorescence microscopy

For widefield microscopy, Zeiss Axio Observer 7 equipped with 100x Plan Apochromat 1.4 NA objective, Colibri 7 LED light source, motorized XYZ stage and PCO.edge 4.2 sCMOS camera was used. Images were acquired at 2x2 or 4x4 binning. Zen blue edition (2.3) software was used for controlling the microscope components and acquisition. For imaging, cells grown in culture media were washed twice with autoclaved dH_2O and resuspended in water. The cell suspension was placed on microscope cover glass and imaged.

Microfluidics assay

Timelapse assays were performed as described (Leontiou et al., 2022).Cell outlines were segmented using the baby algorithm (Pietsch et al., 2023). To quantify the kinetochore retention time of GFP-Bub1 fluorescence, we create a projection of the maximum values from all GFP sections, then divide the median fluorescence of the brightest 5 pixels within each cell by the median fluorescence of the cell as a whole. This ratio reliably measures protein aggregation at an organelle (Leontiou et al., 2022). In the absence of nocodazole, cells with any outlier values for the ratio, defined as values greater than 3 scaled median absolute deviations away from the median, are removed. Cells present for fewer than 80% of recorded time points are also removed. The ratios were normalized for each strain by dividing the mean value for wild-type cells in the absence of nocodazole, measured in the same experiment. To calculate the kinetochore retention times, a threshold of 1.008 was applied to the

ratio values at each time point to determine the presence or absence of Bub1 at the kinetochore. Small gaps in localization (due to kinetochore signal dropping briefly out of focus) were removed by applying a 1-dimensional morphological closing to the thresholded image, with a 3-pixel (3 timepoint or 6 minutes) structuring element. For the temporal heat maps, the data for 30 cells present for the whole experiment are selected for inclusion from each strain pseudo-randomly using the Matlab rand function. There were a small number of outlier values within the heat maps, resulting from a fault in the LED control equipment. These were removed by replacing any values in the 5th percentile of a cell trace with the median value for all time points. The raw data and code used in data processing and plotting are available on request.

Flow cytometry

5 mL of *C. neoformans* culture was grown overnight, and 2 $O.D_{600}$ cells were taken and washed with sterile dH2O and fixed in 1 mL of 70% ethanol overnight at 4°C. Fixed cells were centrifuged at 4000 rpm and washed with 1 mL NS buffer(10 mM Tris-HCl pH 7.5, 250 mM sucrose, 1 mM EDTA (pH 8.0), 1 mM MgCl2, 0.1 mM CaCl2, and 7 mM β-mercaptoethanol) and resuspended in 200 µL of NS buffer added with 2 µg of RNase and incubated at 37°C for 3-4 h. Propidium Iodide (final concentration 12 µg/mL) was added to this mixture and incubated for 30 min at room temperature in the dark. 50 µL of the sample was suspended in 2 mL of 1x PBS (Phosphate buffered saline) solution, vortexed, and sonicated for 10 s at 30% Amp. 30,000 cells were analyzed by flow cytometry using FL2-A channel on (FACSAria III; BD Biosciences) at a rate of 500–2,000 events/s.

Statistics and microscope image analysis

P-values were assessed by unpaired, two-tailed t-test or two-way ANOVA with Tukey's multiple comparison test using GraphPad Prism 8.00 (GraphPad software). Error bars represent the standard deviation (SD) or standard error of the mean (SEM) as mentioned for each experiment. N for each experiment is mentioned in the figure legends. Fiji software (Schindelin et al., 2012) was used to process and analyze microscope images. Fluorescence intensity values of signals were quantified by drawing a circular region of interest (ROI) of defined pixel size on the maximum intensity Z-projected images. The intensity values were calculated by subtracting the

product of mean background fluorescence intensity and area of the ROI from integrated density, and the resultant values were plotted.

Acknowledgments

We thank members of Kaustuv Sanyal lab for their support, discussion, and suggestions on the work. We thank A. Arockia Jeyaprakash, Institute of Cell Biology, School of Biological Sciences, University of Edinburgh, UK, for the discussion and inputs on the work. We thank Ioanna Leontiou (University of Edinburgh) for *bub1Δ* strain construction. We thank the in-house flow cytometry facility at JNCASR and N. Nala for assistance with flow cytometric analysis. We thank Vikas Yadav, Duke University, USA, for the reagents provided for Tub4-mCherry strain construction. Satya Dev Polisetty is a Research Associate supported by DST-TRCII funding by the Government of India. Krishna Bhat is a senior research fellow (SRF) supported by CSIR, Government of India. Kevin Hardwick was supported by the Leverhulme Trust (RPG-2018-379); Ivan Clark was supported by the Wellcome Trust-University of Edinburgh Institutional Strategic Support Fund, and we thank Peter Swain (University of Edinburgh) for leading on this ISSF funding. Kaustuv Sanyal is a JC Bose National Fellow (JCB/2020/000021) of the Science and Engineering Research Board (SERB), Department of Science and Technology, Government of India. Kaustuv Sanyal acknowledges financial support from the Department of Biotechnology, Government of India, SERB, and intramural funding from JNCASR.

Conflict of interest

The authors declare that they have no conflict of interest.

Figure legends

Figure 1. Shugoshin is required for a robust spindle assembly checkpoint arrest. (A) Schematic of the relative positions of the conserved N-terminal coiled-coil domain and the C-terminal basic SGO motif present in Sgo1 of *C. neoformans*. **(B)** A ten-fold serial dilution spotting assay to score for the sensitivity of the CNVY108 (*SGO1 GFP-H4*), CNSD110 (*GFP-H4 sgo1Δ*), SHR741 (*GFP-H4 mad2Δ*), CNSD148 (*GFP-H4 sgo1Δ mad2Δ*) on plates containing the indicated concentrations of thiabendazole (TBZ). No drug represents DMF (dimethyl formamide) only. The plates were incubated at 30°C for 24 h. **(C)** Schematic of the assay to score for cell

cycle arrest phenotypes when treated with nocodazole. Cells treated with nocodazole for 120 and 240 min were scored for cell cycle arrest phenotypes. **(D)** Bar graphs representing the proportion of large-budded cells in the indicated strains, N=3, n>100, cells counted in each experiment. Two-way ANOVA with Tukey's multiple comparison test was used to estimate the significance. ****p<0.0001, ***p<0.001, **p=0.0019/0.0072 and ns=non-significant **(E)** *Left*, an outline of the assay to study the effect of nocodazole on the ploidy content of indicated strains using flow cytometry. *Right*, histograms depicting ploidy changes associated with nocodazole treatment.

Figure 2. Shugoshin ensures Bub1's retention at kinetochores to maintain the spindle assembly checkpoint arrest. (A) Schematic of the SAC pathway and the role of Sgo1 and Aurora B^{Ipl1} in detecting erroneous kinetochore-MT attachments. **(B)** An outline of the experiment used to determine the dynamics of GFP-Bub1 localization under nocodazole-treated conditions. **(C)** Microscopic images of GFP-Bub1 localization in IL102 (*SGO1*) and CNSD176 (*sgo1Δ*). For representation, cells treated with nocodazole for 120 and 280 min were shown. Scale bar, 5 µm. **(D)** Quantification of the proportion of large-budded cells with GFP-Bub1 signal in indicated strains treated with nocodazole. N=3, n>100 cells were analyzed, and the shaded regions above and below the line graphs represent error bands corresponding to SD. **(E)** Quantification of GFP-Bub1 fluorescence intensity values at 120 min post-nocodazole treatment. N=3, n>100 cells analyzed for each experiment. White circles represent the average intensity values of replicates. A mean of the average intensity values of replicates is represented as a black bar, and error bars represent SD. An unpaired t-test was used to test the significance, ** p=0.0092. **(F)** Microfluidics assay to determine the retention time of GFP-Bub1 at kinetochores in response to nocodazole treatment. Kymographs of 30 randomly selected cells are shown. Each bright track on the Y-axis of the kymograph represents GFP-Bub1 signals from an individual cell. The length of each bright track along the X-axis represents the time (min) cells spent in mitosis. Nocodazole (2.5 µg/mL) was added 300 min into the experiment. Assay was performed using IL102 (*GFP-BUB1*), IL143 (*GFP-bub1-kd*), CNSD176 (*GFP-BUB1 sgo1Δ*), CNSD173 (*GFP-bub1-kd sgo1Δ*) and IL089 (*GFP-BUB mad1Δ*) strains. **(G)** Bar graphs representing the quantitative analysis of GFP-Bub1 retention time at kinetochores

obtained from microfluidics assay in the above-indicated strains. n=30, error bars represent SD.

Figure 3. Shugoshin-dependent Aurora B^{Ipl1} pool at kinetochores ensures maintenance of Bub1 to prolong the checkpoint arrest. (A) Microscopic images of Aurora B^{Ipl1}-3xGFP localization in CNSD190 (*AURORA B^{Ipl1}-3xGFP mCherry-CENP-A SGO1*) and CNSD196 (*AURORA B^{Ipl1}-3xGFP mCherry-CENP-A sgo1Δ*) strains treated with nocodazole. For representation, cells treated with nocodazole for 120 and 280 min were shown. Scale bar, 5μm. **(B)** Quantification of the proportion of large-budded cells with Aurora B^{Ipl1}-3xGFP signals in the indicated strains. N=3, n>100 cells were analyzed, and the shaded regions above and below the line graph represent error bands corresponding to SD. **(C)** Quantification of Aurora B^{Ipl1}-3XGFP fluorescence intensity values at 120 min post-nocodazole treatment. N=3, n>58 cells for each experiment. White circles represent the average intensity values of replicates. The mean of the average intensity values of replicates is represented as a black bar. Error bars represent SD. An unpaired t-test was used to test the significance, ** p= 0.0013. **(D)** A schematic to assess the response of Aurora B^{Ipl1} overexpression or depletion to nocodazole treatment. **(E)** Microscopic images of GFP-Bub1 localization in CNSD205 (*GAL7-3xFLAG-AURORA B^{IPL1} GFP-BUB1*) Aurora B^{Ipl1} overexpressed and repressed conditions treated with nocodazole. Cells treated with nocodazole for 120 and 240 min are shown for representation. Scale bar, 5 μm. **(F)** Bar graphs representing the proportion of large-budded cells scored for the presence or absence of GFP-Bub1 signal at 120 and 240 min of nocodazole treatment. n>100 cells were counted. **(G)** Quantification of GFP-Bub1 fluorescence intensity values in Aurora B^{Ipl1} overexpressed and repressed conditions at 120 min of nocodazole treatment. White circles represent the average intensity values of replicates. The mean of the average intensity values of the replicates is represented as a black bar. Error bars represent SD. N=3, n> 79 cells analyzed for each experiment. An unpaired t-test was used to test the significance, *p=0.0439.

Figure 4. Sgo1-mediated Aurora B^{Ipl1} recruitment prevents excess PP1 phosphatase at the kinetochore. (A) The effect of *sgo1Δ* on maintaining a balance between Aurora B^{Ipl1} and PP1 levels at kinetochore in *C. neoformans*. **(B)** Microscopic images of CNKB003 (*GFP-PP1 mCherry-CENP-A*) in *SGO1* and CNSD180 (*GFP-PP1 mCherry-CENP-A sgo1Δ*) cells treated with nocodzole (1

μg/mL) for 120 min. Yellow ovals represent PP1-GFP signals used for quantitation. **(C)** Quantification of GFP-PP1 fluorescence signal intensity values in the above-indicated strains treated with nocodazole. N=3, n>100 cells were analyzed for each experiment. White circles represent the average GFP-PP1 signal intensities calculated for each experimental repeat. An unpaired t-test was used to determine statistical significance. **p= 0.0044. The mean of the average intensity values of replicates is represented as a black bar. Error bars represent SD. **(D)** Microscopic images of CNKB023 (*GFP-PP1 mCherry-CENP-A GAL7-3xFLAG AURORA B*^{IPL1}) Aurora B^{Ipl1} overexpressed and repressed conditions treated with nocodazole (1 μg/mL) for 120 min. **(E)** Quantification of fluorescence intensity values of GFP-PP1 signal in the conditions mentioned above. N=4, n=100 cells for each experiment. White circles represent the average intensity values of replicates. Error bars represent SD. The mean of the average intensity values plotted is represented as a black bar. Paired t-test was used to determine statistical significance. **p= 0.0069.

Figure 5. The kinase activity of Bub1 is dispensable for shugoshin-mediated maintenance of the spindle assembly checkpoint. (A) Schematic of the conserved pathway of shugoshin recruitment to kinetochores by the kinase activity of Bub1 and the role of Sgo1 in *C. neoformans* in SAC maintenance. **(B)** A ten-fold serial dilution spotting assay to score for the sensitivity of the CNSD110 (*sgo1Δ*), IL143 (*GFP-bub1-kd*), CNSD173 (*sgo1Δ GFP-bub1-kd*) double mutants and SHR866 (*mad2Δ*) to thiabendazole. **(C)** *Top*, experimental strategy used to test the requirement of the lysine, K382 residue of Sgo1 in the SAC maintenance function. *Below*, a ten-fold serial dilution spotting assay to score for the sensitivity of the CNSD110 (*sgo1Δ*), CNSD207 (*sgo1Δ GFP-SGO1-SH1*), and CNSD209 (*sgo1Δ GFP-sgo1-K382A-SH1*).

Figure 6. Kinetochore proximal association of Sgo1 in MT-depolymerizing conditions. (A-D) *Left,* microscopic images of GFP-Sgo1 localized with a kinetochore marker, CENP-A, and an SPB marker, Tub4, at different stages of the mitotic cell cycle, in nocodazole treated and Cdc20 depletion conditions. Scale bar, 5 μm. **(A)** CNSD125 (*GFP-SGO1 mCherry-CENP-A*). **(B)** CNSD130 (*GFP-SGO1 TUB4-mCherry*). **(C)** Nocodazole (1 μg/mL) treated condition. *Top panel*, CNSD125. *Bottom panel*, CNSD130. **(D)** Cdc20 depletion condition, CNSD167 (*GFP-SGO1 mCherry-CENP-A GAL7-3xFLAG-CDC20*). *Right*, line scan profiles of both GFP

(Sgo1) and mCherry (CENP-A, Tub4) fluorescence signals. Distance on the X-axis represents the length of the line drawn on the image to measure fluorescence intensity. Gray values on the Y-axis represent the fluorescence signal intensity. **(E)** Kinetochore proximal model of Sgo1 function in SAC maintenance in *C. neoformans.*

Supplementary figure legends

Supplementary figure 1. *C. neoformans* Sgo1 has a conserved coiled-coil domain and the SGO motif. (A) The protein sequence of *C. neoformans* Sgo1. **(B)** Multiple sequence alignment (MSA) of the CnSgo1 N-terminal coiled-coil and the C-terminal SGO motif with vertebrate and invertebrate species (Cn- *C. neoformans*; Sc- *Saccharomyces cerevisiae*; Sp- *Schizosaccharomyces pombe*; Hs- *Homo sapiens*; Mm- *Mus musculus*; Xl- *Xenopus laevis*; Dm- *Drosophila melanogaster*). Multiple sequence alignment of Sgo1 homologs was performed using Clustal Omega (Sievers et al., 2011), and the alignment was formatted using Jalview 2 (Waterhouse et al., 2009). *Represent amino acid residues involved in PP2A binding. The dark blue circle represents the key residue (K382 in *C. neoformans*) required for Bub1-mediated kinetochore proximal centromere localization of shugoshin. The teal blue colored box represents the coiled-coil domain. The light blue colored box represents the conserved basic SGO motif. **(C)** Microscopic images of GFP-H4 tagged CNVY108 (*SGO1 MAD2*), CNSD117 (*sgo1Δ*), SHR866 (*mad2Δ*), CNSD148 (*sgo1Δ mad2Δ*) treated with nocodazole (1 µg/mL) for 120- and 240-min. Scale bar, 5 µm. **(D)** Bar graphs representing the proportion of unbudded, small-budded, large-budded, and tri-budded cells. N=3, n>100 cells counted in each experiment. **(E)** Bar graphs representing the proportion of large-budded cells of indicated phenotypes, N=3, n>100 cells counted in each experiment.

Supplementary figure 2. *sgo1Δ bgi1Δ* double mutant cells exhibit enhanced sensitivity to MT depolymerizing drug. A ten-fold serial dilution spotting assay to score for the sensitivity of the wild-type CNVY108 (*SGO1 BGI1 GFP-H4*), CNSD117 (*sgo1Δ GFP-H4)*, SHR741 (*mad2Δ GFP-H4*), SHR830 (*bgi1Δ GFP-H4*), CNSD148 (*sgo1Δ mad2Δ GFP-H4*) and CNSD163 (*sgo1Δ bgi1Δ GFP-H4*) to thiabendazole. No drug represents DMF (Dimethyl formamide) only. The plates were incubated at 30°C for 24 h.

Supplementary figure 3. Aurora B^{Ipl1} colocalizes with the kinetochore (CENP-A) during G2 and mitosis and exhibits spindle-like localization. (A) Microscopic images of Aurora B^{Ipl1}-3xGFP localized with mCherry-CENP-A at G2, metaphase, and anaphase stages of the cell cycle. **(B)** Colocalization of Aurora B^{Ipl1}-3xGFP with mCherry-CENP-A when treated with nocodazole (1 µg/mL) for 120 min. Scale bar, 5 µm.

Supplementary figure 4. Aurora B^{Ipl1} mutants fail to arrest at metaphase in response to nocodazole treatment. (A) Microscopic images of CNNV104 (*GFP-H4 GAL7-AURORA B^{IPL1}*) grown in permissive and non-permissive media in the presence and absence of nocodazole. Scale bar, 5 µm. Representative images of cells treated with nocodazole and depleted of Aurora B^{Ipl1} for 240 and 480 min were shown. **(B)** *Left*, bar graphs representing the proportion of unbudded, small-budded, large-budded, and tri-budded cells. *Right*, bar graphs representing the proportion of large-budded cells of indicated phenotype, n>100 cells counted for each time point.

Supplementary figure 5. Sequence conservation of *C. neoformans* PP1. Multiple sequence alignment of PP1 homolog of *C. neoformans* (CNAG_03706) with vertebrate and invertebrate species (Cn- *C. neoformans*; Sc- *S. cerevisiae*; Sp- *S. pombe*; Ca- *Candida albicans*; Hs- *H. sapiens*; Mm- *M. musculus*; Dm- *D. melanogaster*) was performed using Clustal Omega (Sievers et al., 2011) and the alignment was formatted using Jalview 2 (Waterhouse et al., 2009). Highly conserved regions are shaded in dark blue.

Supplementary figure 6. Shugoshin responds to tensionless kinetochore-MT attachments. (A) Pairwise sequence alignment of Scc1 homologs of *C. neoformans* (CNAG_01023) and *S. cerevisiae* by Clustal Omega (Sievers et al., 2011), and formatted using Jalview 2 (Waterhouse et al., 2009). Highly conserved regions are shaded in dark blue. The two domains corresponding to N- and C-terminal Scc1 domains (E-values of 2.0e-31 and 2.2e-15, respectively) of CnScc1 are highlighted in violet and green boxes. **(B)** Schematic of the domains present in *C. neoformans* Scc1 protein. **(C)** Plate photographs of strains expressing Scc1 under the regulatable *GAL7* promoter grown in media containing glucose (non-permissive) and galactose (permissive). **(D)** Schematic to check the response of Scc1 repression in *SGO1* and *sgo1Δ* backgrounds. **(E)** Microscopic images of GFP-H4 tagged CNSD181 (*GAL7-*

3xFLAG-SCC1) and CNSD182 (*sgo1Δ GAL7-3xFLAG-SCC1*) strains depleted of Scc1. Representative images of cells depleted of Scc1 for 4 and 6 h were shown. Scale bar, 5 µm. **(F)** Bar graphs representing the percentage of unbudded, small-budded, large-budded, and tri-budded cells scored. N=2, n>100 cells for each experiment, error bars represent SD.

Supplementary figure 7. Schematic highlighting the sub-cellular localization of shugoshin reported in various species. *Left*, schematic highlighting the spatial positioning of SPB/centrosome and centromeres in yeasts and metazoans. *Right*, localization of the shugoshin with respect to the kinetochore, MTOCs equivalent to centrosomes or SPBs, spindle MTs, and telomeres. Filled and open squares represent the presence or absence of shugoshin at the indicated sub-cellular locations. The data was compiled from reviews (Marston, 2015, Gutierrez-Caballero et al., 2012). [1,2] (Mohr et al., 2015, Wang et al., 2008), [3*] (Salic et al., 2004), this study has shown that the purified N-terminal region of shugoshin is capable of binding to MTs *in* vitro. [4] (Sane et al., 2021) and [5] (Tashiro et al., 2016).

865 **Table S1: List of strains**

Strain	Genotype	Source
H99	*MATα* (wild-type)	(Perfect et al., 1993)
CNVY101	*MATa::mCherry-CENP-A-NEO (pLKB74)*	(Kozubowski et al., 2013)
CNVY108	*MATα::GFP-H4-NAT (pVY3)*	(Kozubowski et al., 2013)
SHR741	*MATα::GFP-H4-NAT (pVY3) MAD2::mad2-NEO*	(Sridhar et al., 2021)
SHR830	*MATα::GFP-H4-NAT (pVY3) BGI1::bgi1Δ-HygB*	(Sridhar et al., 2021)
IL143	*MATα::BUB1::bub1Δ-NAT HISp-GFP-bub1-kd-HYGB (chromosome 3, safe haven p37)*	(Leontiou et al., 2022)
IL102	*MATα::BUB1::bub1Δ-NAT HISp-GFP-bub1-HygB (chromosome 3, safe haven p37)*	(Leontiou et al., 2022)
IL089	*MATα::MAD1::mad1Δ HISp:GFP-Bub1: HygB (chromosome 3, safe haven p37)*	(Leontiou et al., 2022)
CNNV113	*MATα:: AUR B^{IPL1}:: AUR B^{IPL1}p- AUR B^{IPL1}-3xGFP-NEO*	(Varshney et al., 2019)
CNNV104	*MATα:GFP-H4-NAT (pVY3), AUR B^{IPL1}::GAL7p- AUR B^{IPL1}- HygB*	(Varshney et al., 2019)
CNSD110	*MATα::SGO1::sgo1Δ-NEO*	This Study
CNSD117	*MATα::GFP-H4-NAT (pVY3) SGO1::sgo1Δ-NEO*	This Study
CNSD125	*MATa::mCherry-CENP-A-NEO (pLKB74) SGO1::SGO1pr-GFP-SGO1-NAT (pSD10)*	This study
CNSD127	*MATα::SGO1::SGO1p-GFP-SGO1-NAT (pSD10)*	This study
CNSD130	*MATα::SGO1::SGO1p-GFP-SGO1-NAT (pSD10) TUB4::TUB4-mCherry-NEO*	This study
CNSD148	*MATα::GFP-H4-NAT (pVY3) MAD2::mad2-NEO SGO1::sgo1Δ-NEO*	This study
CNSD163	*MATα::GFP-H4-NAT (pVY3) BGI1::bgi1Δ-HygB SGO1::sgo1Δ-NEO*	This study
CNSD167	*MATa::mCherry-CENP-A-NEO (pLKB74) SGO1::SGO1pr-GFP-SGO1-NAT (pSD10) CDC20p::GAL7p-3xFLAG-CDC20-HYGB*	This study
CNSD173	*MATα::BUB1::bub1Δ-NAT HISp-GFP-bub1-kd- HygB (chromosome 3, safe haven p37) SGO1::sgo1Δ-NEO*	This study
CNSD176	*MATα::BUB1::bub1Δ-NAT HISp-GFP-bub1-*	This study

	HygB (chromosome 3, safe haven p37) SGO1::sgo1Δ-NEO	
CNSD180	*MATa::mcherry-CENP-A-NEO PP1:: PP1p-GFP-PP1-NAT* (pKB004) *SGO1::sgo1Δ-HYGB*	This study
CNSD181	*MATα::GFP-H4-NAT (pVY3) SCC1p::GAL7p-3xFLAG-SCC1- HygB*	This study
CNSD182	*MATα::GFP-H4-NAT (pVY3) SCC1p::GAL7p-3xFLAG-SCC1- HygB SGO1::sgo1Δ-NEO*	This study
CNSD190	*MATα::AUR B^{IPL1}:: AUR B^{IPL1}p- AUR B^{IPL1}-3xGFP-NEO mCherry-CENP-A- HygB (pLKB71)*	This study
CNSD196	*MATα:: AUR B^{IPL1}:: AUR B^{IPL1}p- AUR B^{IPL1}-3xGFP-NEO mCherry-CENP-A-HygB (pLKB71) SGO1::sgo1Δ-NAT*	This study
CNSD205	*MATα::BUB1::bub1Δ-NAT HISp-GFP-bub1-HygB (chromosome 3, safe haven p37) AUR B^{IPL1}::GAL7-3XFLAG-AUR B^{IPL1}-NEO*	This study
CNSD207	*MATα::SGO1::sgo1Δ-NEO SGO1p-GFP-SGO1- HygB (pSD34) (SAFE HAVEN1, chrormosome1)*	This study
CNSD209	*MATα::SGO1::sgo1Δ-NEO SGO1p-GFP-sgo1-K382A- HygB (pSD35) (SAFE HAVEN1, chrormosome1)*	This study
CNKB003	*MATa::mcherry-CENP-A-NEO PP1:: PP1p-GFP-PP1-NAT* (pKB004)	This study
CNKB023	*MATa::mcherry-CENP-A-NEO PP1:: PP1p-GFP-PP1-NAT* (pKB004) *AUR B^{IPL1}::GAL7-3XFLAG-AUR B^{IPL1}-NEO*	This study

Table S2: List of plasmids

Plasmid	Description	Source
pVY7	*H3p-GFP-NAT* from pCN19 cloned into pBSII using SacI-ApaI	(Yadav and Sanyal, 2018)
pSH7G	*HygB-GAL7-GFP* pBlueScriptII KS(-)	(Sridhar et al., 2021)
pLKB71	pXLI + *mCherry-CENP-A-HygB*	From Joseph Heitman, Duke University, US
pSD10	*H3p* of pVY7 replaced with *SGO1p* (SacI/NcoI) + *SGO1* homology region (BamHI)	This study
pSD29	*GAL7p of p*SH7G replaced with *SGO1p* (SpeI/BamHI)+*SGO1* 3'UTR (NheI/ApaI)+*SAFE HAVEN1* (ApaI)	This study
pSD34	*SGO1* allele (HpaI/NheI) cloned into pSD29	This study
pSD35	*sgo1-K382A* allele (HpaI/NheI) cloned into pSD29	This study
pKB004	*H3p* of pVY7 replaced with *PP1p* (SacI/NcoI) +*PP1* homology region (SpeI)	This study

894 **Table S3: List of primers**

Primer number	Sequence 5'-3'	Purpose
SDP1	CCGATGAGCGTACACCACTTAC	*SGO1* deletion overlap primers
SDP2	CCAGCTCACATCCTCGCAGCTGCTACGAGATTGAGACGAATG	
SDP3	CATTCGTCTCAATCTCGTAGCAGCTGCGAGGATGTGAGCTGG	
SDP4	CTCCCAACTTCCCCGCTTTTGGTTTATCTGTATTAACACGGAAGAG	
SDP5	CTCTTCCGTGTTAATACAGATAAACCAAAAGCGGGGAAGTTGGGAG	
SDP6	ATCAGAACGCACGTCGCAC	
SDP7	CAGGCAGAGGATTGGGAAGTC	
SDP8	CCAGTTCCTCAAAGAGCTTGAC	*SGO1* deletion confirmation primer
SDP20	ACTGAGCTCACTATCTGCAAAATCGACTTG	*SGO1pr-GFP-SGO1* N-terminal tagging
SDP21	CATGCCATGGCCTGTATTTACGCCTGGAG	
SDP22	CGCGGATCCATGTCCCAGAGGCAAGGCAG	
SDP23	CGCGGATCCGTTTCATCTCGACCACAGGTC	
SDP24	GGCACAAGCTGGAGTACAAC	Universal forward primer for tagging confirmation
SDP25	CTTCAGGTTCAGCATTGTCTG	
SDP27	ACTGGGCCCACACGATGTTTTCCATCAG	*SAFE HAVEN1* cloning
SDP28	ACTGGGCCCGGTCTCACAATCATCAACATC	
SDP54	AACAGTGATGGCAGCGTC	*TUB4-mCherry* C-terminal tagging overlap
SDP55	CGCATCCAACGTCATCCAAG	
VYP360	CTTGTGAACAATGCTGATAGTGTGG	
VYP361	CTCGCCCTTGCTCACCATCTCCCCCCCAAAATCGATATAATCC	
VYP362	GGATTATATCGATTTTGGGGGGGAGATGGTGAGCAAGGGCGAG	
VYP363	CGAAGTGCGTACTTGAAAGAAGTCCAAGCTTGGTACCGAGCTC	
VYP364	GAGCTCGGTACCAAGCTTGGACTTCTTTCAAGTACGCACTTCG	
VYP365	TGATGATCTCCAAGCTCTTCAC	
SDP108	TTGTTGTTACCATCATCCTCTC	Universal confirmation Reverse primer for deletion cassettes
SDP110	AGATCGACAACATGCGACC	*GAL7-3xFLAG-*

SDP111	CTGCAGATATCCATCACACTGGGAAGGGACC GTTTTTGACTAAC	*Cdc20* tagging overlap
SDP112	GTTAGTCAAAAACGGTCCCTTCCCAGTGTGA TGGATATCTGCAG	
SDP113	ATGGTCTTTGTAGTCCATCATTCTCAGGAGA GAATTGAGTG	
SDP114	ATGGACTACAAAGACCATGACGGTGATTATA AAGATC ATGACATCGACTACAAGGATGACGATGACAA GCTTGGAGA ACATACATCTGGC	
SDP115	CCGTGCCAACTCATGACC	
SDP116	GGATGTCGGCAATGAATTCAG	*GAL7-3xFLAG-Cdc20* integration confirmation
SDP162	AGCCTCATCCGACTTCACAG	*GAL7-3xFLAG-SCC1* tagging overlap
SDP163	GCAGATATCCATCACACTGGCCAACACGTAC ACGTCAACC	
SDP164	GGTTGACGTGTACGTGTTGGCCAGTGTGATG GATATCTGC	
SDP165	CACCGTCATGGTCTTTGTAGTCCATTCTCAG GAGAGAATTG AGTGC	
SDP166	ATGGACTACAAAGACCATGACGGTGATTATA AAGATCATGA CATCGACTACAAGGATGACGATGACAAGATC TTGAACGAAC TGATCAAGTC	
SDP167	CCATCTCGACATCATAGTCGTC	
SDP168	CCTTACGACCACAACCAGC	*GAL7-3xFLAG-SCC1* integration confirmation
SDP191	TATGACCTAGAACTGACAGACTCG	*GAL7-3xFLAG-AUR B^{IPL1} tagging overlap*
SDP192	GCAGATATCCATCACACTGGGGAGGCCAAAT CTGGAGG	
SDP193	CCTCCAGATTTGGCCTCCCCAGTGTGATGGA TATCTGC	
SDP195	ATGGACTACAAAGACCATGACGGTGATTATA AAGATCATGACATCGACTACAAGGAT GACGATGACAAGTCCTCGCAGAATGTTTCTG G	

SDP196	CTCGTCAAATCTGCCTAATCTGG	
SDP197	GTCCTGTAGAAGTTGAATTGC	*GAL7-3xFLAG-AUR B*^{IPL1} integration confirmation
SDP170	TTCGTCGACAACGCTAGCTAATGGCGACGATAATGATG	*SGO1* 3'UTR cloning for complementation
SDP171	TATGGGCCCTGCACTTGCGATAGATATCG	
SDP172	ACTGTTAACATGTCCCAGAGGCAAGGC	*SGO1* gene amplification for sgo1 deletion complementation
SDP173	GTTGCTAGCTTACTGCAAGACTCCAACGGC	
SDP198	CCCATCAGGTTTCCGCATGGCTCTTTCGAAATTATCAGCTAACG	*sgo1-K382A* allele amplification for sgo1 deletion complementation
SDP199	CGTTAGCTGATAATTTCGAAAGAGCCATGCGGAAACCTGATGGG	
SDP201	CTGAAGGAACTGGAAGAGG	*sgo1-K382A* sequencing primer
KBP001	ACGGAGCTCGACGTCGTACAAATGCATAC	*GFP-PP1* N-terminal tagging
KBP002	GGCCCATGGTTTATACGAAGTACGTTATATGTG	
KBP003	TATACTAGTATGGGAGAACAGCCTGAAATTG	
KBP005	ATCACTAGTCAATAAACAAGCTCACTTGGAAGG	
KBP006	GCCGCCGTATCCACCGTATTTC	

References

AKTAR, K., DAVIES, T., LEONTIOU, I., CLARK, I., SPANOS, C., WALLACE, E., TUCK, L., JEYAPRAKASH, A. A. & HARDWICK, K. G. 2023. *mps1* and *mad* mutations reduce Cryptococcus neoformans titan cell viability. *bioRxiv*, 2023.04.09.536157.

BIGGINS, S. & MURRAY, A. W. 2001. The budding yeast protein kinase Ipl1/Aurora allows the absence of tension to activate the spindle checkpoint. *Genes Dev,* 15**,** 3118-29.

BOYARCHUK, Y., SALIC, A., DASSO, M. & ARNAOUTOV, A. 2007. Bub1 is essential for assembly of the functional inner centromere. *J Cell Biol,* 176**,** 919-28.

CHEESEMAN, I. M., CHAPPIE, J. S., WILSON-KUBALEK, E. M. & DESAI, A. 2006. The conserved KMN network constitutes the core microtubule-binding site of the kinetochore. *Cell,* 127**,** 983-97.

CIFERRI, C., PASQUALATO, S., SCREPANTI, E., VARETTI, G., SANTAGUIDA, S., DOS REIS, G., MAIOLICA, A., POLKA, J., DE LUCA, J. G., DE WULF, P., SALEK, M., RAPPSILBER, J., MOORES, C. A., SALMON, E. D. & MUSACCHIO, A. 2008. Implications for kinetochore-microtubule attachment from the structure of an engineered Ndc80 complex. *Cell,* 133**,** 427-39.

CLARKE, A. S., TANG, T. T., OOI, D. L. & ORR-WEAVER, T. L. 2005. POLO kinase regulates the Drosophila centromere cohesion protein MEI-S332. *Dev Cell,* 8**,** 53-64.

COHEN-FIX, O., PETERS, J. M., KIRSCHNER, M. W. & KOSHLAND, D. 1996. Anaphase initiation in Saccharomyces cerevisiae is controlled by the APC-dependent degradation of the anaphase inhibitor Pds1p. *Genes Dev,* 10**,** 3081-93.

DAVIDSON, R. C., CRUZ, M. C., SIA, R. A., ALLEN, B., ALSPAUGH, J. A. & HEITMAN, J. 2000. Gene disruption by biolistic transformation in serotype D strains of Cryptococcus neoformans. *Fungal Genet Biol,* 29**,** 38-48.

ESPEUT, J., CHEERAMBATHUR, D. K., KRENNING, L., OEGEMA, K. & DESAI, A. 2012. Microtubule binding by KNL-1 contributes to spindle checkpoint silencing at the kinetochore. *J Cell Biol,* 196**,** 469-82.

FERNIUS, J. & HARDWICK, K. G. 2007. Bub1 kinase targets Sgo1 to ensure efficient chromosome biorientation in budding yeast mitosis. *PLoS Genet,* 3**,** e213.

FUNABIKI, H., HAGAN, I., UZAWA, S. & YANAGIDA, M. 1993. Cell cycle-dependent specific positioning and clustering of centromeres and telomeres in fission yeast. *J Cell Biol,* 121**,** 961-76.

GUACCI, V., KOSHLAND, D. & STRUNNIKOV, A. 1997. A direct link between sister chromatid cohesion and chromosome condensation revealed through the analysis of MCD1 in S. cerevisiae. *Cell,* 91**,** 47-57.

GUTIERREZ-CABALLERO, C., CEBOLLERO, L. R. & PENDAS, A. M. 2012. Shugoshins: from protectors of cohesion to versatile adaptors at the centromere. *Trends Genet,* 28**,** 351-60.

HARDWICK, K. G., JOHNSTON, R. C., SMITH, D. L. & MURRAY, A. W. 2000. MAD3 encodes a novel component of the spindle checkpoint which interacts with Bub3p, Cdc20p, and Mad2p. *J Cell Biol,* 148**,** 871-82.

943 HAUF, S., COLE, R. W., LATERRA, S., ZIMMER, C., SCHNAPP, G., WALTER, R., HECKEL, A., VAN MEEL, J.,
944 RIEDER, C. L. & PETERS, J. M. 2003. The small molecule Hesperadin reveals a role for Aurora
945 B in correcting kinetochore-microtubule attachment and in maintaining the spindle assembly
946 checkpoint. *J Cell Biol,* 161**,** 281-94.

947 HINDRIKSEN, S., LENS, S. M. A. & HADDERS, M. A. 2017. The Ins and Outs of Aurora B Inner
948 Centromere Localization. *Front Cell Dev Biol,* 5**,** 112.

949 HWANG, L. H., LAU, L. F., SMITH, D. L., MISTROT, C. A., HARDWICK, K. G., HWANG, E. S., AMON, A. &
950 MURRAY, A. W. 1998. Budding yeast Cdc20: a target of the spindle checkpoint. *Science,* 279**,**
951 1041-4.

952 INDJEIAN, V. B., STERN, B. M. & MURRAY, A. W. 2005. The centromeric protein Sgo1 is required to
953 sense lack of tension on mitotic chromosomes. *Science,* 307**,** 130-3.

954 KALLIO, M. J., MCCLELAND, M. L., STUKENBERG, P. T. & GORBSKY, G. J. 2002. Inhibition of aurora B
955 kinase blocks chromosome segregation, overrides the spindle checkpoint, and perturbs
956 microtubule dynamics in mitosis. *Curr Biol,* 12**,** 900-5.

957 KAWASHIMA, S. A., YAMAGISHI, Y., HONDA, T., ISHIGURO, K. & WATANABE, Y. 2010.
958 Phosphorylation of H2A by Bub1 prevents chromosomal instability through localizing
959 shugoshin. *Science,* 327**,** 172-7.

960 KING, R. W., DESHAIES, R. J., PETERS, J. M. & KIRSCHNER, M. W. 1996. How proteolysis drives the cell
961 cycle. *Science,* 274**,** 1652-9.

962 KITAJIMA, T. S., KAWASHIMA, S. A. & WATANABE, Y. 2004. The conserved kinetochore protein
963 shugoshin protects centromeric cohesion during meiosis. *Nature,* 427**,** 510-7.

964 KOZUBOWSKI, L., YADAV, V., CHATTERJEE, G., SRIDHAR, S., YAMAGUCHI, M., KAWAMOTO, S., BOSE,
965 I., HEITMAN, J. & SANYAL, K. 2013. Ordered kinetochore assembly in the human-pathogenic
966 basidiomycetous yeast Cryptococcus neoformans. *mBio,* 4**,** e00614-13.

967 LARA-GONZALEZ, P., PINES, J. & DESAI, A. 2021. Spindle assembly checkpoint activation and silencing
968 at kinetochores. *Semin Cell Dev Biol,* 117**,** 86-98.

969 LEONTIOU, I., DAVIES, T., CLARK, I., AKTAR, K., SURESH, A. P., ABAD, M. A., SPANOS, C., LEE, K.-T.,
970 BAHN, Y.-S., JEYAPRAKASH, A. A. & HARDWICK, K. G. 2022. Bub1 kinase acts as a signalling
971 hub for the entire Cryptococcus neoformans spindle assembly checkpoint pathway. *bioRxiv***,**
972 2022.09.21.508923.

973 LESAGE, B., QIAN, J. & BOLLEN, M. 2011. Spindle checkpoint silencing: PP1 tips the balance. *Curr Biol,*
974 21**,** R898-903.

975 LIU, D., VLEUGEL, M., BACKER, C. B., HORI, T., FUKAGAWA, T., CHEESEMAN, I. M. & LAMPSON, M. A.
976 2010. Regulated targeting of protein phosphatase 1 to the outer kinetochore by KNL1
977 opposes Aurora B kinase. *J Cell Biol,* 188**,** 809-20.

978 LIU, H., JIA, L. & YU, H. 2013. Phospho-H2A and cohesin specify distinct tension-regulated Sgo1 pools
979 at kinetochores and inner centromeres. *Curr Biol,* 23**,** 1927-33.

980 MARSTON, A. L. 2015. Shugoshins: tension-sensitive pericentromeric adaptors safeguarding
981 chromosome segregation. *Mol Cell Biol,* 35**,** 634-48.

982 MEADOWS, J. C., SHEPPERD, L. A., VANOOSTHUYSE, V., LANCASTER, T. C., SOCHAJ, A. M., BUTTRICK,
983 G. J., HARDWICK, K. G. & MILLAR, J. B. 2011. Spindle checkpoint silencing requires
984 association of PP1 to both Spc7 and kinesin-8 motors. *Dev Cell,* 20**,** 739-50.

985 MICHAELIS, C., CIOSK, R. & NASMYTH, K. 1997. Cohesins: chromosomal proteins that prevent
986 premature separation of sister chromatids. *Cell,* 91**,** 35-45.

987 MOHR, L., BUHEITEL, J., SCHOCKEL, L., KARALUS, D., MAYER, B. & STEMMANN, O. 2015. An
988 Alternatively Spliced Bifunctional Localization Signal Reprograms Human Shugoshin 1 to
989 Protect Centrosomal Instead of Centromeric Cohesin. *Cell Rep,* 12**,** 2156-68.

990 MUSACCHIO, A. 2015. The Molecular Biology of Spindle Assembly Checkpoint Signaling Dynamics.
991 *Curr Biol,* 25**,** R1002-18.

992 MUSACCHIO, A. & DESAI, A. 2017. A Molecular View of Kinetochore Assembly and Function. *Biology*
993 *(Basel),* 6.

994 MUSACCHIO, A. & SALMON, E. D. 2007. The spindle-assembly checkpoint in space and time. *Nat Rev*
995 *Mol Cell Biol,* 8**,** 379-93.

996 NIJENHUIS, W., VALLARDI, G., TEIXEIRA, A., KOPS, G. J. & SAURIN, A. T. 2014. Negative feedback at
997 kinetochores underlies a responsive spindle checkpoint signal. *Nat Cell Biol,* 16**,** 1257-64.

998 OHKUSU, M., RACLAVSKY, V. & TAKEO, K. 2004. Induced synchrony in Cryptococcus neoformans
999 after release from G2-arrest. *Antonie Van Leeuwenhoek,* 85**,** 37-44.

1000 PERFECT, J. R., KETABCHI, N., COX, G. M., INGRAM, C. W. & BEISER, C. L. 1993. Karyotyping of
1001 Cryptococcus neoformans as an epidemiological tool. *J Clin Microbiol,* 31**,** 3305-9.

1002 PETERSEN, J. & HAGAN, I. M. 2003. S. pombe aurora kinase/survivin is required for chromosome
1003 condensation and the spindle checkpoint attachment response. *Curr Biol,* 13**,** 590-7.

1004 PIETSCH, J. M. J., MUNOZ, A. F., ADJAVON, D. A., FARQUHAR, I., CLARK, I. B. N. & SWAIN, P. S. 2023.
1005 Determining growth rates from bright-field images of budding cells through identifying
1006 overlaps. *Elife,* 12.

1007 PINSKY, B. A., KUNG, C., SHOKAT, K. M. & BIGGINS, S. 2006. The Ipl1-Aurora protein kinase activates
1008 the spindle checkpoint by creating unattached kinetochores. *Nat Cell Biol,* 8**,** 78-83.

1009 PINSKY, B. A., NELSON, C. R. & BIGGINS, S. 2009. Protein phosphatase 1 regulates exit from the
1010 spindle checkpoint in budding yeast. *Curr Biol,* 19**,** 1182-7.

1011 ROSENBERG, J. S., CROSS, F. R. & FUNABIKI, H. 2011. KNL1/Spc105 recruits PP1 to silence the spindle
1012 assembly checkpoint. *Curr Biol,* 21**,** 942-7.

1013 ROY, B., HAN, S. J. Y., FONTAN, A. N., JEMA, S. & JOGLEKAR, A. P. 2022. Aurora B phosphorylates
1014 Bub1 to promote spindle assembly checkpoint signaling. *Curr Biol,* 32**,** 237-247 e6.

1015 ROY, B., VERMA, V., SIM, J., FONTAN, A. & JOGLEKAR, A. P. 2019. Delineating the contribution of
1016 Spc105-bound PP1 to spindle checkpoint silencing and kinetochore microtubule attachment
1017 regulation. *J Cell Biol,* 218**,** 3926-3942.

1018 SALIC, A., WATERS, J. C. & MITCHISON, T. J. 2004. Vertebrate shugoshin links sister centromere
1019 cohesion and kinetochore microtubule stability in mitosis. *Cell,* 118**,** 567-78.

1020 SANE, A., SRIDHAR, S., SANYAL, K. & GHOSH, S. K. 2021. Shugoshin ensures maintenance of the
1021 spindle assembly checkpoint response and efficient spindle disassembly. *Mol Microbiol,* 116**,**
1022 1079-1098.

1023 SANTAGUIDA, S., VERNIERI, C., VILLA, F., CILIBERTO, A. & MUSACCHIO, A. 2011. Evidence that Aurora
1024 B is implicated in spindle checkpoint signalling independently of error correction. *EMBO J,*
1025 30**,** 1508-19.

1026 SAURIN, A. T., VAN DER WAAL, M. S., MEDEMA, R. H., LENS, S. M. & KOPS, G. J. 2011. Aurora B
1027 potentiates Mps1 activation to ensure rapid checkpoint establishment at the onset of
1028 mitosis. *Nat Commun,* 2**,** 316.

1029 SCHINDELIN, J., ARGANDA-CARRERAS, I., FRISE, E., KAYNIG, V., LONGAIR, M., PIETZSCH, T.,
1030 PREIBISCH, S., RUEDEN, C., SAALFELD, S., SCHMID, B., TINEVEZ, J. Y., WHITE, D. J.,
1031 HARTENSTEIN, V., ELICEIRI, K., TOMANCAK, P. & CARDONA, A. 2012. Fiji: an open-source
1032 platform for biological-image analysis. *Nat Methods,* 9**,** 676-82.

1033 SIEVERS, F., WILM, A., DINEEN, D., GIBSON, T. J., KARPLUS, K., LI, W., LOPEZ, R., MCWILLIAM, H.,
1034 REMMERT, M., SODING, J., THOMPSON, J. D. & HIGGINS, D. G. 2011. Fast, scalable
1035 generation of high-quality protein multiple sequence alignments using Clustal Omega. *Mol*
1036 *Syst Biol,* 7**,** 539.

1037 SRIDHAR, S., HORI, T., NAKAGAWA, R., FUKAGAWA, T. & SANYAL, K. 2021. Bridgin connects the outer
1038 kinetochore to centromeric chromatin. *Nat Commun,* 12**,** 146.

1039 SUDAKIN, V., CHAN, G. K. & YEN, T. J. 2001. Checkpoint inhibition of the APC/C in HeLa cells is
1040 mediated by a complex of BUBR1, BUB3, CDC20, and MAD2. *J Cell Biol,* 154**,** 925-36.

1041 TANAKA, T. U., RACHIDI, N., JANKE, C., PEREIRA, G., GALOVA, M., SCHIEBEL, E., STARK, M. J. &
1042 NASMYTH, K. 2002. Evidence that the Ipl1-Sli15 (Aurora kinase-INCENP) complex promotes
1043 chromosome bi-orientation by altering kinetochore-spindle pole connections. *Cell,* 108**,** 317-
1044 29.

1045 TASHIRO, S., HANDA, T., MATSUDA, A., BAN, T., TAKIGAWA, T., MIYASATO, K., ISHII, K., KUGOU, K.,
1046 OHTA, K., HIRAOKA, Y., MASUKATA, H. & KANOH, J. 2016. Shugoshin forms a specialized
1047 chromatin domain at subtelomeres that regulates transcription and replication timing. *Nat*
1048 *Commun,* 7**,** 10393.

1049 TATCHELL, K., MAKRANTONI, V., STARK, M. J. & ROBINSON, L. C. 2011. Temperature-sensitive ipl1-
1050 2/Aurora B mutation is suppressed by mutations in TOR complex 1 via the Glc7/PP1
1051 phosphatase. *Proc Natl Acad Sci U S A,* 108**,** 3994-9.

1052 VAN HOOFF, J. J., TROMER, E., VAN WIJK, L. M., SNEL, B. & KOPS, G. J. 2017. Evolutionary dynamics
1053 of the kinetochore network in eukaryotes as revealed by comparative genomics. *EMBO Rep,*
1054 18**,** 1559-1571.

1055 VANOOSTHUYSE, V. & HARDWICK, K. G. 2009. A novel protein phosphatase 1-dependent spindle
1056 checkpoint silencing mechanism. *Curr Biol,* 19**,** 1176-81.

1057 VANOOSTHUYSE, V., PRYKHOZHIJ, S. & HARDWICK, K. G. 2007. Shugoshin 2 regulates localization of
1058 the chromosomal passenger proteins in fission yeast mitosis. *Mol Biol Cell,* 18**,** 1657-69.

1059 VARSHNEY, N., SOM, S., CHATTERJEE, S., SRIDHAR, S., BHATTACHARYYA, D., PAUL, R. & SANYAL, K.
1060 2019. Spatio-temporal regulation of nuclear division by Aurora B kinase Ipl1 in Cryptococcus
1061 neoformans. *PLoS Genet,* 15**,** e1007959.

1062 WANG, X., YANG, Y., DUAN, Q., JIANG, N., HUANG, Y., DARZYNKIEWICZ, Z. & DAI, W. 2008. sSgo1, a
1063 major splice variant of Sgo1, functions in centriole cohesion where it is regulated by Plk1.
1064 *Dev Cell,* 14**,** 331-41.

1065 WATERHOUSE, A. M., PROCTER, J. B., MARTIN, D. M., CLAMP, M. & BARTON, G. J. 2009. Jalview
1066 Version 2--a multiple sequence alignment editor and analysis workbench. *Bioinformatics,* 25**,**
1067 1189-91.

1068 XU, Z., CETIN, B., ANGER, M., CHO, U. S., HELMHART, W., NASMYTH, K. & XU, W. 2009. Structure and
1069 function of the PP2A-shugoshin interaction. *Mol Cell,* 35**,** 426-41.

1070 YADAV, V. & SANYAL, K. 2018. Sad1 Spatiotemporally Regulates Kinetochore Clustering To Ensure
1071 High-Fidelity Chromosome Segregation in the Human Fungal Pathogen Cryptococcus
1072 neoformans. *mSphere,* 3.

1073 ZICH, J. & HARDWICK, K. G. 2010. Getting down to the phosphorylated 'nuts and bolts' of spindle
1074 checkpoint signalling. *Trends Biochem Sci,* 35**,** 18-27.

1075

Figure 1. Polisetty et. al

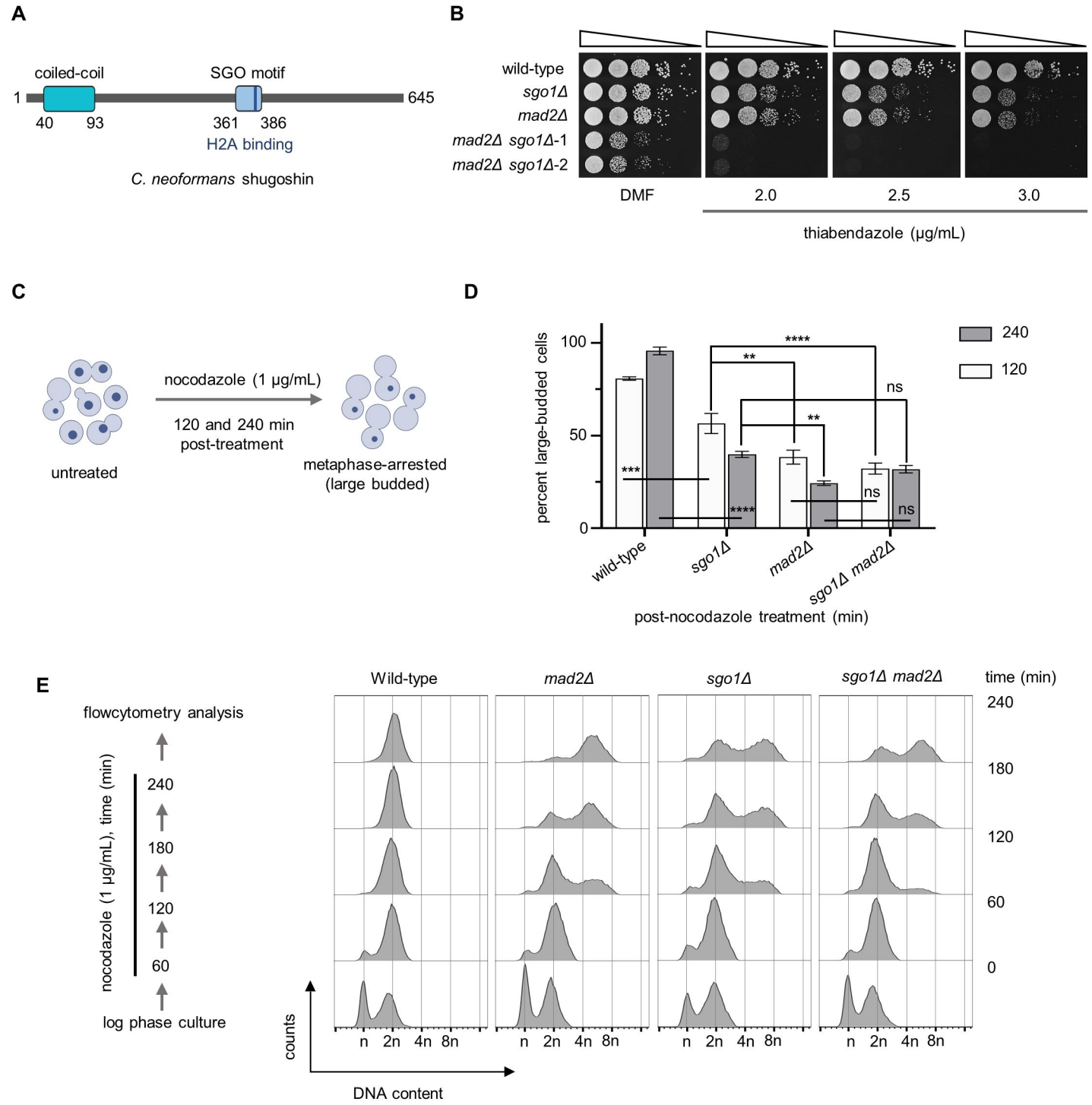

Figure 2. *Polisetty et. al*

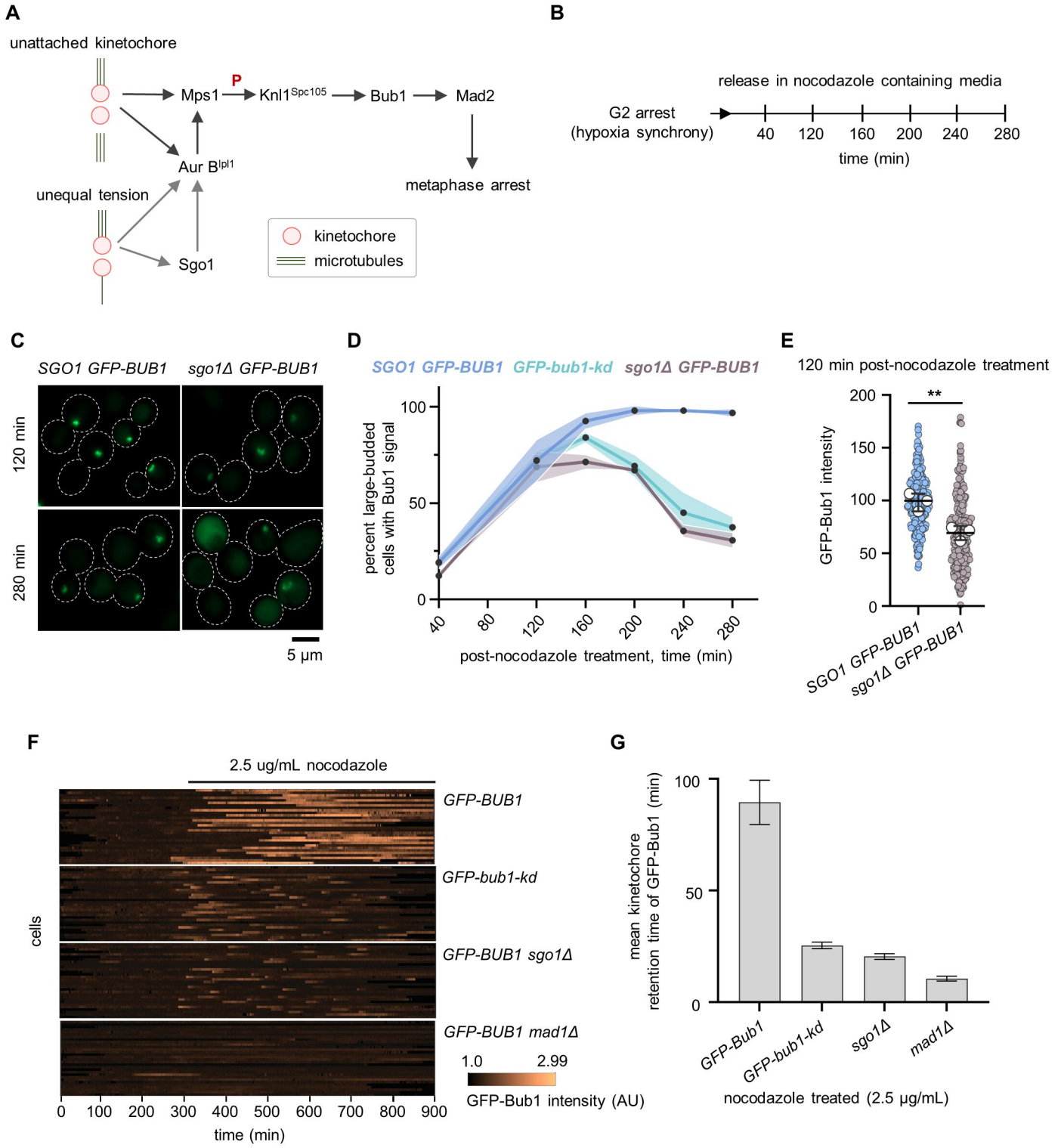

Figure 3. *Polisetty et. al*

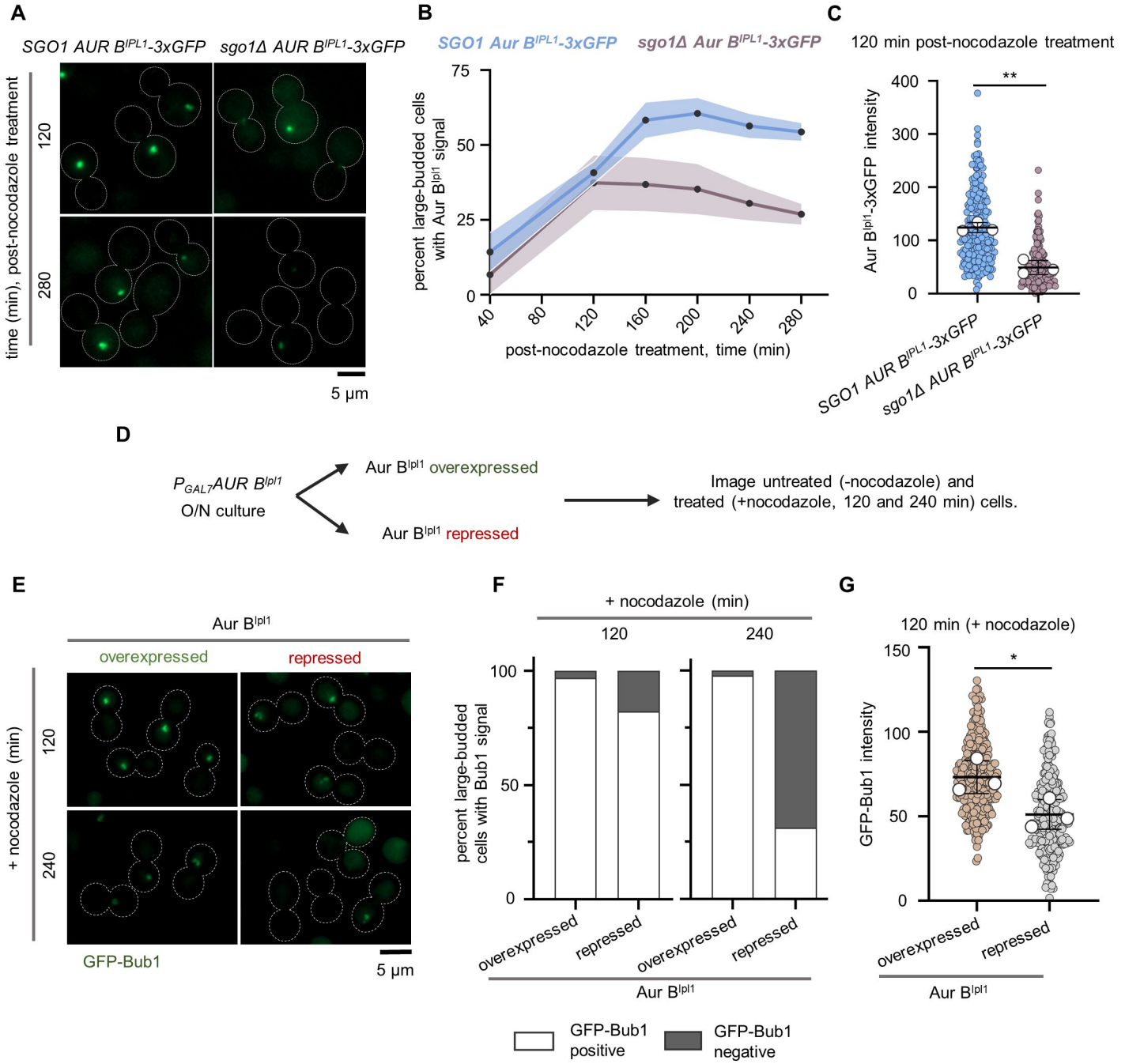

Figure 4. *Polisetty et. al*

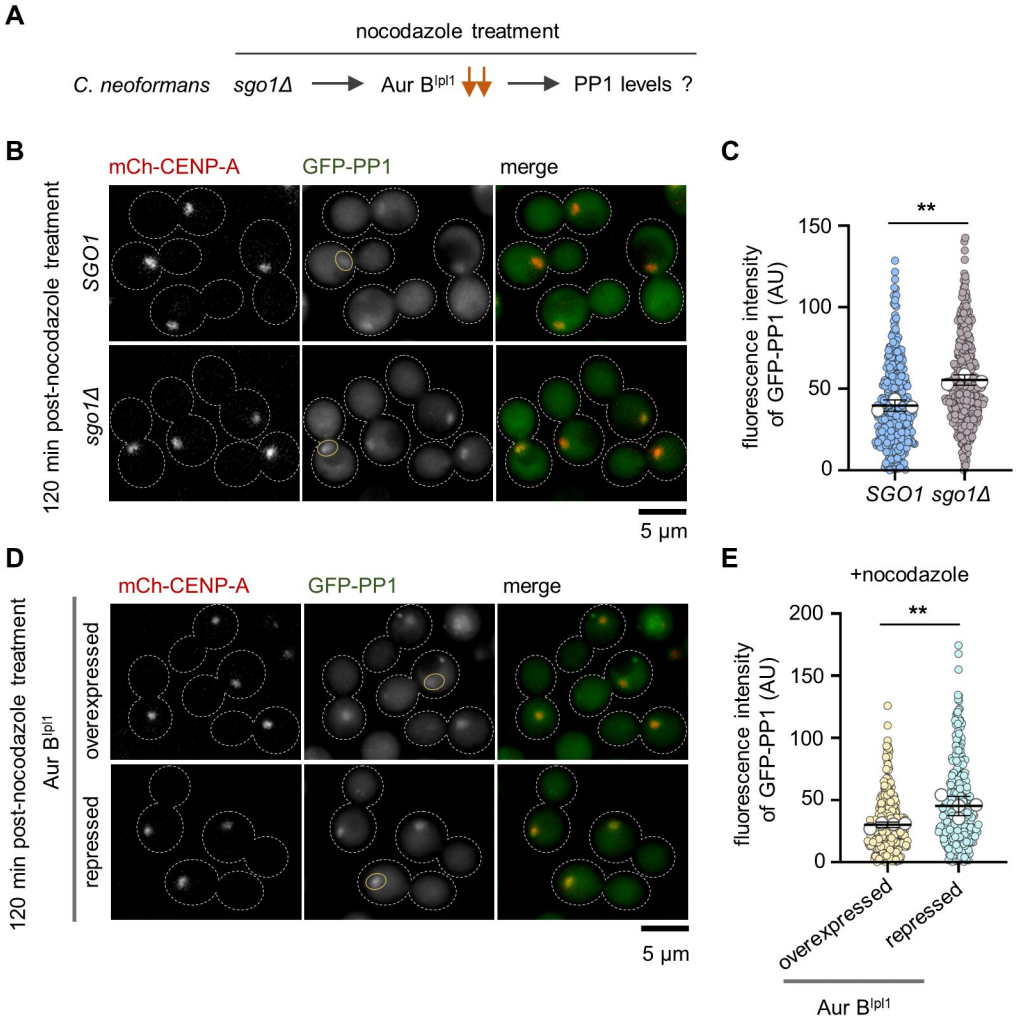

Figure 5. *Polisetty et. al*

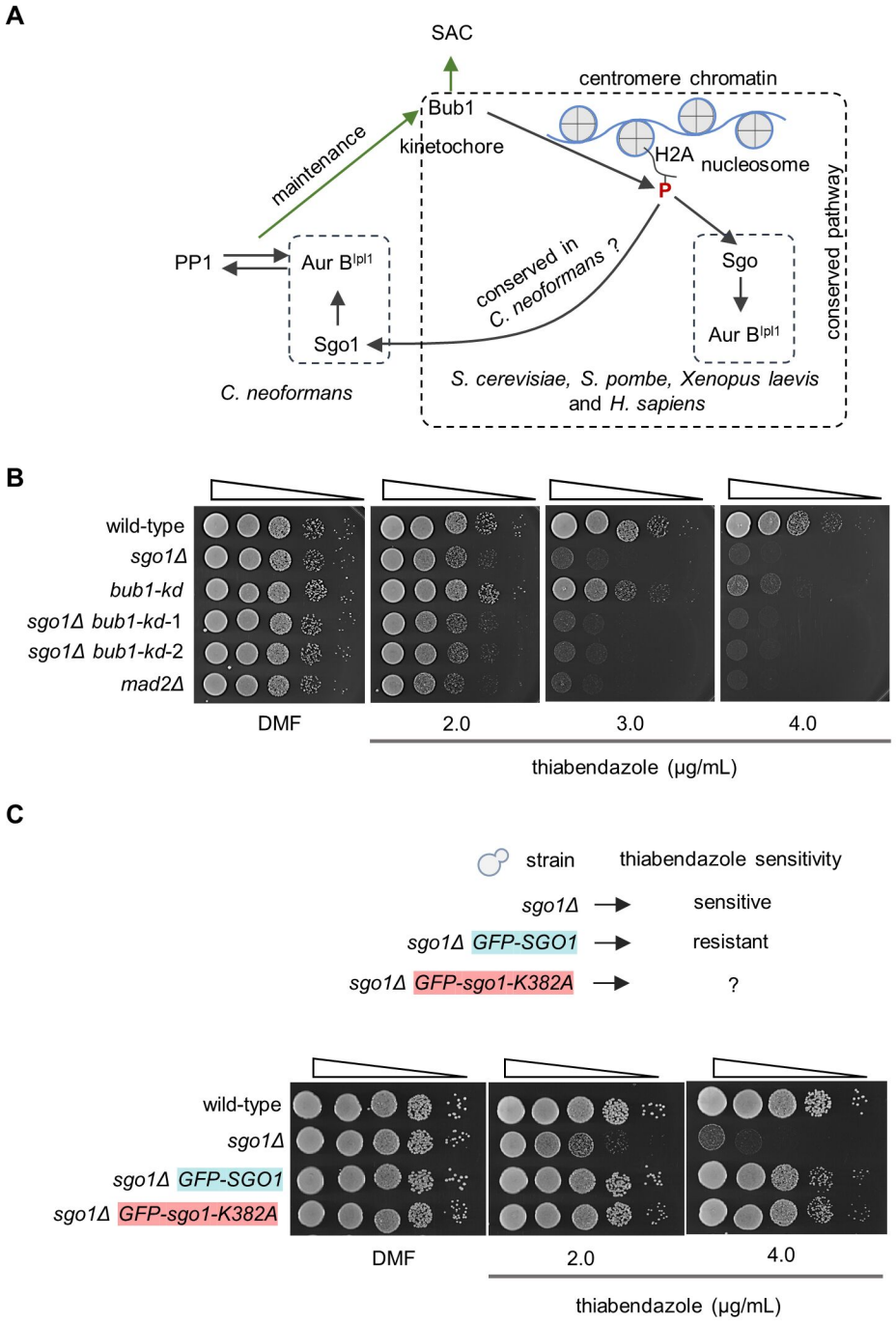

Figure 6. *Polisetty et. al*

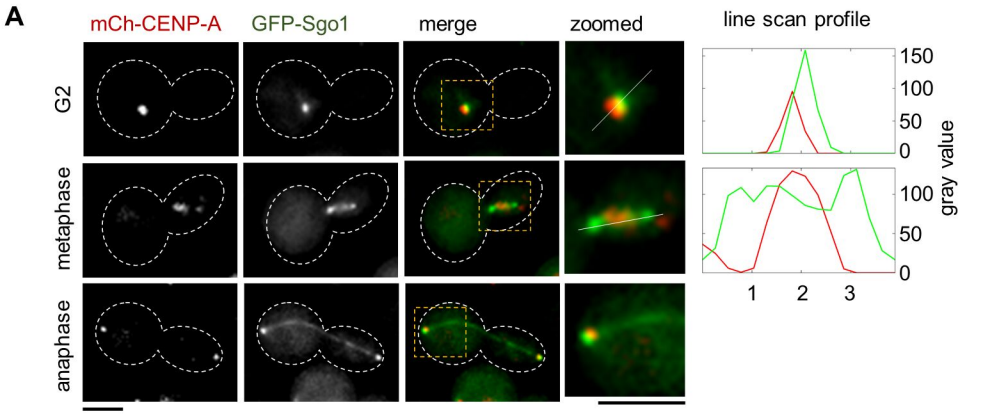

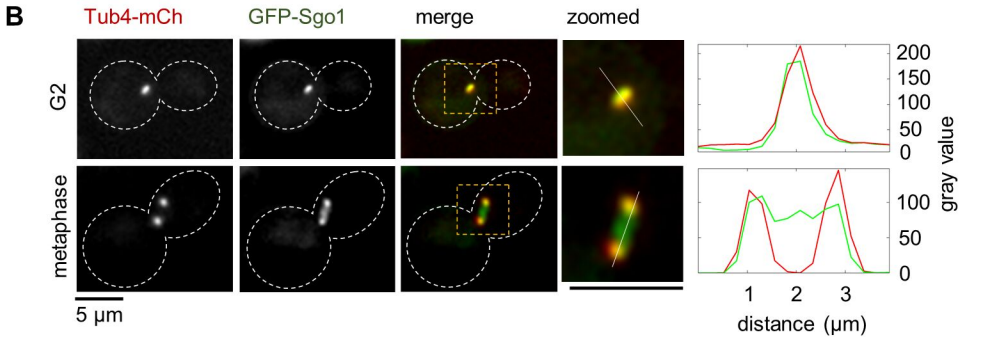

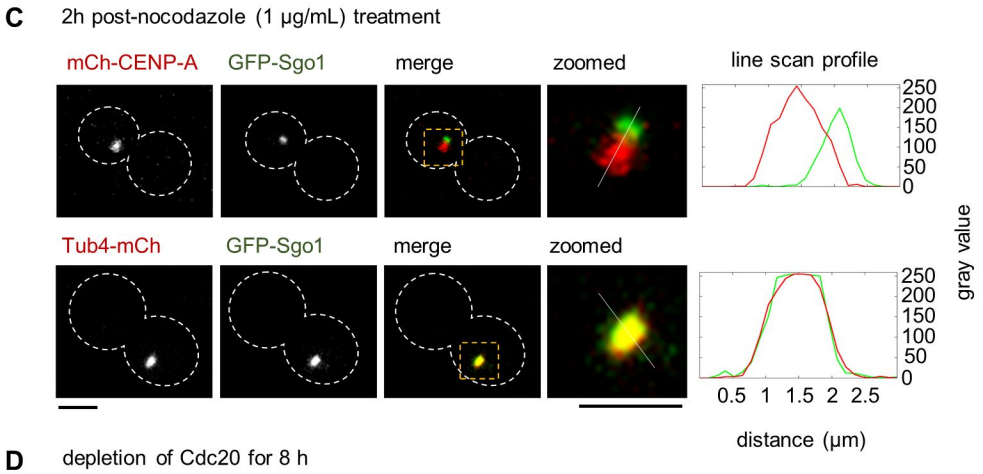

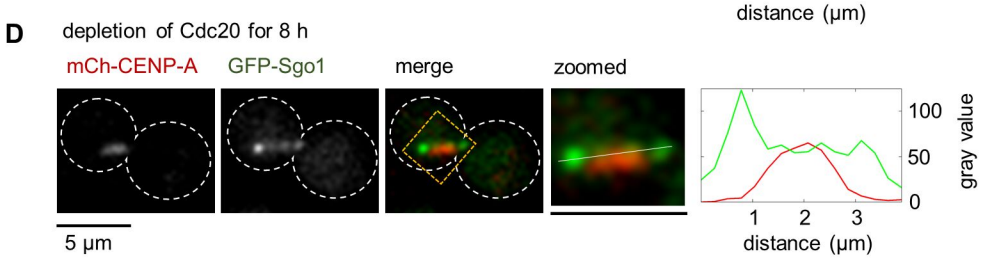

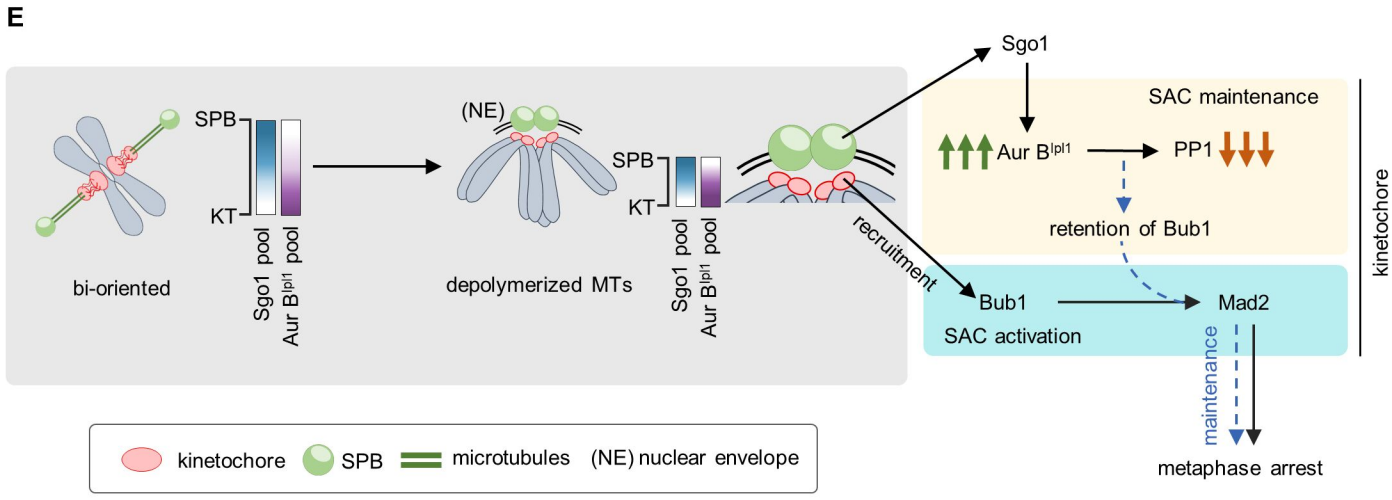

Supplementary Figure 1. *Polisetty et. al*

A *C. neoformans* Sgo1 (CnSgo1)

```
  1 MSQRQGRRSTGPTPLPQQTSQERREQGFVEQQKFDDFRRRHREQNKDIILDNVERRKIIKTLQDEISILQNELLDVRRRNMALESRVKKMERENSRLGGASVLK 104
105 ALDHLLAAAPALYSLRQSLSSLPTPPPSASYKQPSNTRPTLTFVGNPTATRPAANGKQRQDLGAVVESEEGEWMDDRRVTSRSRGRGRQTDVGSVAASRSPRPK 208
209 TPVFPARSSVSPSPKKVISARKIPVKRRRESGLLSARPRSCSPEVVNGQEPVIPVKQEPQVVDKEPVGETRVDEEPVGETSEWEEGPVVEMKPDEALALVQEEE 312
313 QVDFSRKEKEGNTEAEAEIVEVNETGEPESEPSRPSDPAITDNAEPEGTGRGRRARASVVSYKEPSLVKKMRKPDGIQTQDVIKTLTRKSISPRRAKSSLSPKR 416
417 TKKDAYTTSSPPPIPLIPERSPSSRSASTRTANLSASSQSMRRKSTLPKANNRSRGKQEEVGKMARGEDKGGEDLEEYEDIHDDGEELDLKFGRSLQIGTGSGF 520
521 RKPSSSSTLSHHPAMRSNAPKTLPTTSVPATTLMSAPLPANKVDSLLAALNVDPRPVRSTGTGVTTSSRRQSSARGFRPTSTMRSRDVLTEVRPSNVETKPALE 624
625 QDLKKDAGEVARGTRAVGVLQ                                                                                   645
```

B

```
                 *   *  *
CnSgo1  41 --HREQNKDIILDNVERRKIIKTLQDEISILQNELLDVRRRNMALESRVKKMERENSRLGGASVLKALDHLL-- 110
ScSgo1  47 --YSRQNSLLAKDNSILKIKVNSLEKKISQLVQENVTLRSKTSISEAIYR------ERLS--NQLQVIENGIIQ 110
SpSgo2  17 --QIRQYKEIIRISKAQSIRIKELQLENERLLSENIDLRTTAINLEEQLETVQNENEENK--TKLAALLNRFHE  86
HsSgo1  55 KNYQDNNKMLVLALENEKSKVKEAQDIILQLRKECYYLTCQLYALKGKLTSQQTVE------------------ 110
MmSgo1  55 RYYQDNNRLLVLALENEKSKVREAQDVILQLRKECYYLTCQLYALKEKLTSRQSE------------------ 110
XlSgo1  55 KNYKANNTALALALEAEKLKTRQAQDLILGLKREHQRLIFEIFMLRRRLQSQQGRD------------------ 110
DmSgo1   7 QCYKLLNAELMDQVQKQRLEIGEYRKRVISLEREIMDIREEHVLQN--------HRQRMENISIVRSLMLSLNV  72
```

Coiled-coil

```
CnSgo1 360 -GTGRGRRARASVVSYKEPSLVKKMRKPDGIQTQ 392
ScSgo1 364 -SFTRTRRTRGKAVDYTLPSLRAKMRRPSEKLVD 396
SpSgo2 568 KPDGRSRRE-RKKVNYALPGLRTKLRRNFDLPSD 600
HsSgo1 470 -AVALPKRRCTASVNYKEPTLASKLRRGDPFT-- 500
MmSgo1 460 -AVALTKRRCSTIKSYKEPTLASKLRRGDPFTDL 492
XlSgo1 597 -STPSRKRRCKVSINYAEPKLSGKLRRGDPFTDS 629
DmSgo1 367 -NSARPSRSCR-PTSLVEPSLKNKLRNGSKGKAK 398
```

SGO motif

C

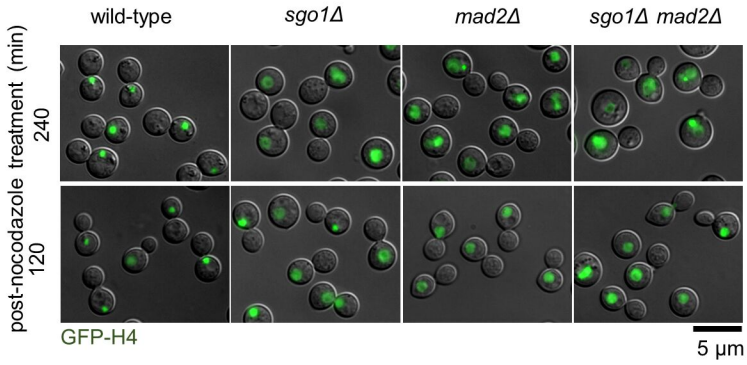

D

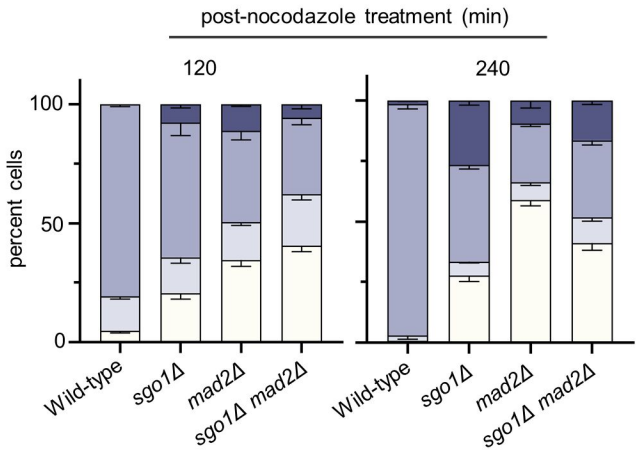

E

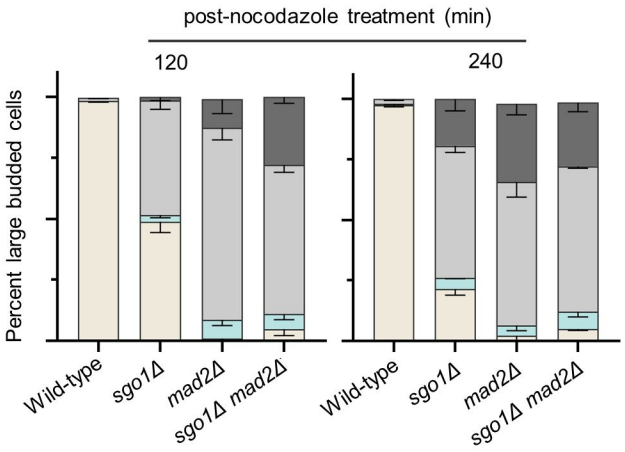

Supplementary Figure 2. *Polisetty et. al*

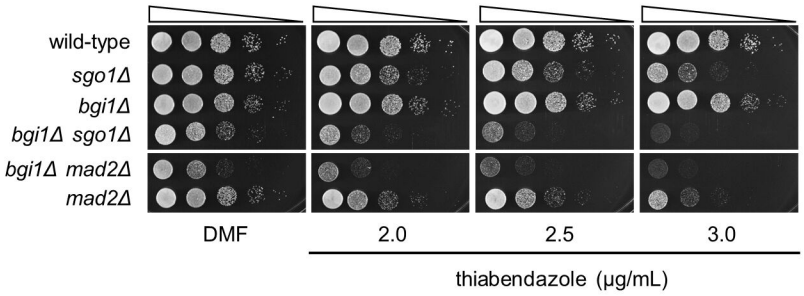

Supplementary Figure 3. ***Polisetty et. al***

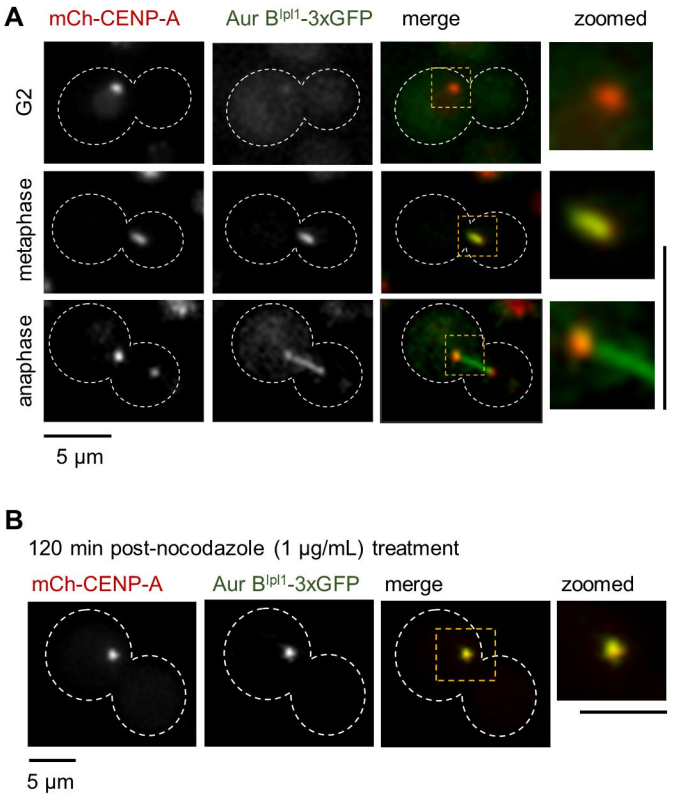

Supplementary Figure 4. ***Polisetty et. al***

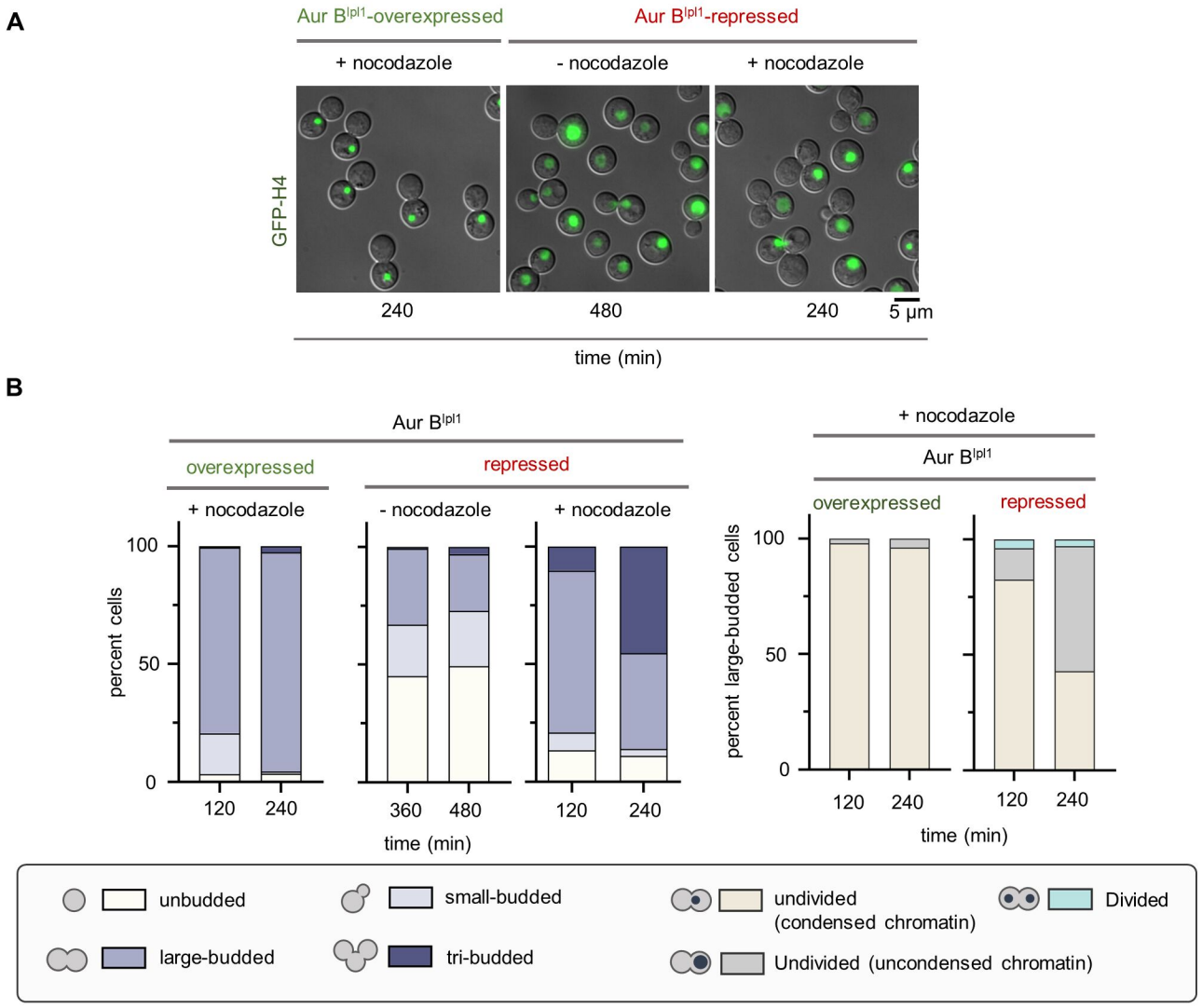

Supplementary Figure 5. ***Polisetty et. al***

```
                    10        20        30        40        50        60        70        80        90
CnPP1     1 ---MGEQPEIDLDSVIDRLLEVRGNRPGKAVQLAEYEIKYLCTKAREIFISQPILLELEAPIKICGDIHGQYYDLLRLFEYGGFPPEANYLFLGDYVDRG  97
ScGlc7    1 ----MDSQPVDVDNIIDRLLEVRGSKPGQQVDLEENEIRYLCSKARSIFIKQPILLELEAPIKICGDIHGQYYDLLRLFEYGGFPPESNYLFLGDYVDRG  96
SpDis12   1 ----MSNPDVDLDSIIDRLLEVRGSRPGRQVQLSEDEIRFLCNKAREIFISQPILLELEAPLKICGDIHGQYYDLLRLFEYGGFPPEANYLFLGDYVDRG  96
CaPP1     1 MSNNIEDDSISVDNIVDRLLEVRGSRPGKQVTLTENEIRFLCTKAREIFIQQPILLELEAPIKICGDIHGQYYDLLRLFEYGGFPPEANYLFLGDYVDRG 100
HsPP1γ    1 ---MADLDKLNIDSITQRLLEVRGSKPGKNVQLQENEIRGLCLKSREIFLSQPILLELEAPLKICGDIHGQYYDLLRLFEYGGFPPESNYLFLGDYVDRG  97
MmPP1γ    1 ---MADIDKLNIDSIIQRLLEVRGSKPGKNVQLQENEIRGLCLKSREIFLSQPILLELEAPLKICGDIHGQYYDLLRLFEYGGFPPESNYLFLGDYVDRG  97
DmPP1γ    1 -----MGDVMNIDSIISRLLEVRGARPGKNVQLSEGEIRGLCLKSREIFLSQPILLELEAPLKICGDIHGQYYDLLRLFEYGGFPPESNYLFLGDYVDRG  95

                   110       120       130       140       150       160       170       180       190
CnPP1    98 KQSLETICLLLAYKIKYPENFFIILRGNHECASINRIYGFYDECKRRYNIKLWKTFTDCFNCLPIAAIIDEKIFTMHGGLSPDLQSMEQIRRVMRPTDVPD 197
ScGlc7   97 KQSLETICLLLAYKIKYPENFFIILRGNHECASINRIYGFYDECKRRYNIKLWKTFTDCFNCLPIAAIIDEKIFCMHGGLSPDLNSMEQIRRVMRPTDIPD 196
SpDis12  97 KQSLEVICLLLAYKIKYPENFFIILRGNHECASINRIYGFYDECKRRYNIKLWKTFTDCFNCLPIAAIIDEKIFTMHGGLSPDLNSMDQIQRIMRPTDVPD 196
CaPP1   101 KQSLETICLLLAYKIKYPENFFIILRGNHECASINRIYGFYDECKRRFNIKLWKTFTDCFNCLPIAAIIDEKIFTMHGGLSPDLNSMEQIRRVMRPTDIPD 200
HsPP1γ   98 KQSLETICLLLAYKIKYPENFFLLRGNHECASINRIYGFYDECKRRYNIKLWKTFTDCFNCLPIAAIVDEKIFCCHGGLSPDLQSMEQIRRIMRPTDVPD 197
MmPP1γ   98 KQSLETICLLLAYKIKYPENFFLLRGNHECASINRIYGFYDECKRRYNIKLWKTFTDCFNCLPIAAIVDEKIFCCHGGLSPDLQSMEQIRRIMRPTDVPD 197
DmPP1γ   96 KQSLETICLLLAYKIKYSENFFLLRGNHECASINRIYGFYDECKRRYSIKLWKTFTDCFNCLPVAAIVDEKIFCCHGGLSPDLTSMEQIRRIMRPTDVPD 195

                   210       220       230       240       250       260       270       280       290
CnPP1   198 TGLLCDLLWSDPDKDITGWSENDRGVSFTFGPDVVSRFLQKHDMDLICRAHQVVEDGYEFFAKRQLVTLFSAPNYCGEFDNAGAMMSVDDTLLCSFQILK 297
ScGlc7  197 VGLLCDLLWSDPDKDIVGWSENDRGVSFTFGPDVVNRFLQKQDMELICRAHQVVEDGYEFFSKRQLVTLFSAPNYCGEFDNAGAMMSVDESLLCSFQILK 296
SpDis12 197 TGLLCDLLWSDPDKDLTGWGDNDRGVSFTFGPDVVSRFLHKHDMDLVCRAHQVVEDGYEFFSKRQLVTLFSAPNYCGEFDNAGAMMSVDESLLCSFQILK 296
CaPP1   201 VGLLCDLLWSDPDKDITGWSENDRGVSFTFGPDVVSRFLQKHDMDLICRAHQVVEDGYEFFSKRQLVTLFSAPNYCGEFDNAGAMMSVDESLLCSFQILK 300
HsPP1γ  198 QGLLCDLLWSDPDKDVLGWGENDRGVSFTFGAEVVAKFLHKHDLDLICRAHQVVEDGYEFFAKRQLVTLFSAPNYCGEFDNAGAMMSVDETLMCSFQILK 297
MmPP1γ  198 QGLLCDLLWSDPDKDVLGWGENDRGVSFTFGAEVVAKFLHKHDLDLICRAHQVVEDGYEFFAKRQLVTLFSAPNYCGEFDNAGAMMSVDETLMCSFQILK 297
DmPP1γ  196 QGLLCDLLWSDPDKDTMGWGENDRGVSFTFGAEVVAKFLQKHEFDLICRAHQVVEDGYEFFAKRMLVTLFSAPNYCGEFDNAGAMMSVDDTLMCSFQILK 295

                   310       320       330
CnPP1   298 PAEKKPKYGGYGGSARR-------------- 314
ScGlc7  297 PAQKSLPRQAGGRKKK---------------- 312
SpDis12 297 PAEKKQRYGYQGSSQNWHMTPPRKNKTGNSK 327
CaPP1   301 PADKKPRYAPANVANNRPGANQRKPKKAVK- 330
HsPP1γ  298 PAEKKKPNATRPVTPPRGMITKQAKK----- 323
MmPP1γ  298 PAEKKKPNATRPVTPPRGMITKQAKK----- 323
DmPP1γ  296 PADKRKK------------------------ 302
```

Supplementary Figure 6. *Polisetty et. al*

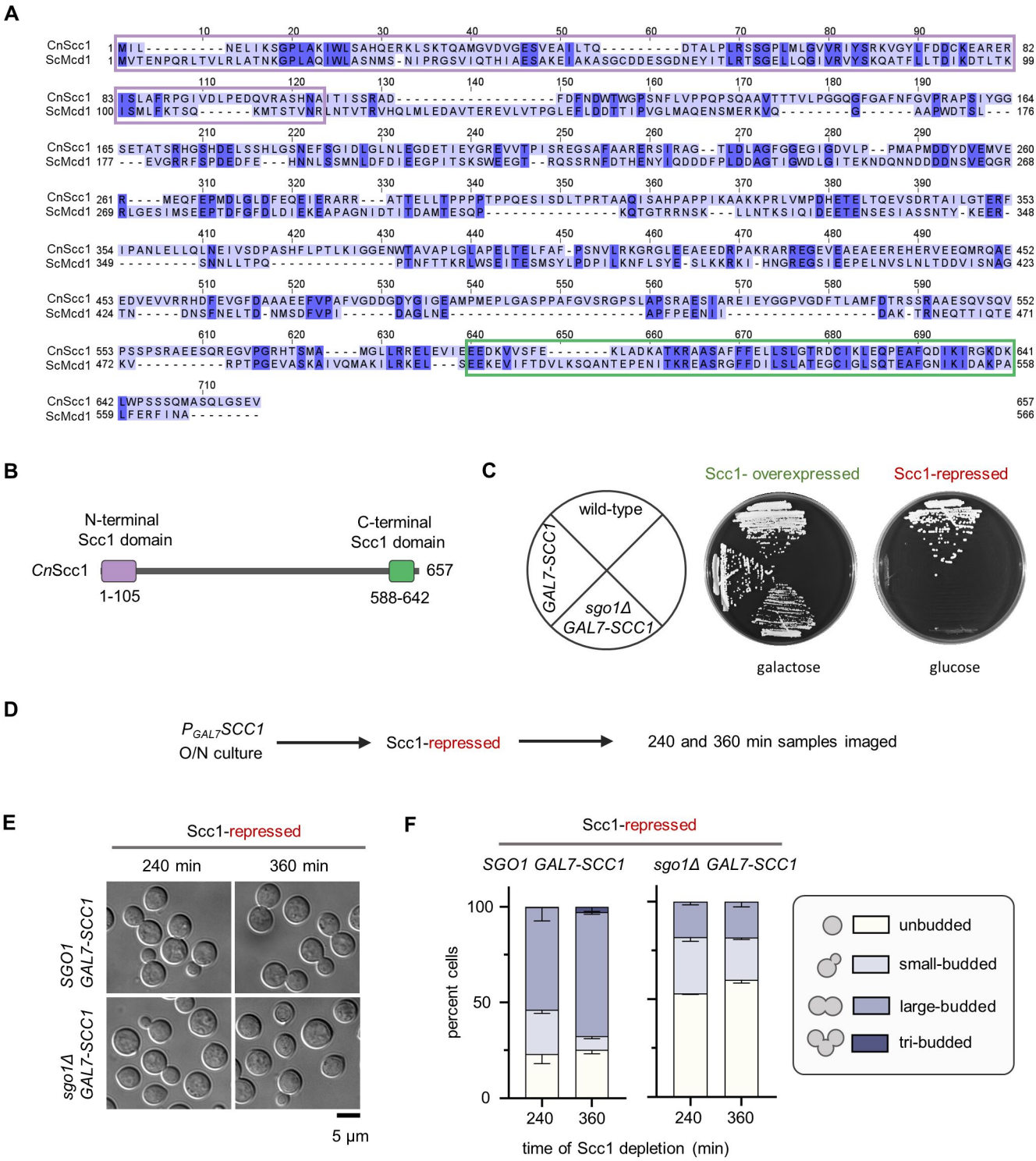
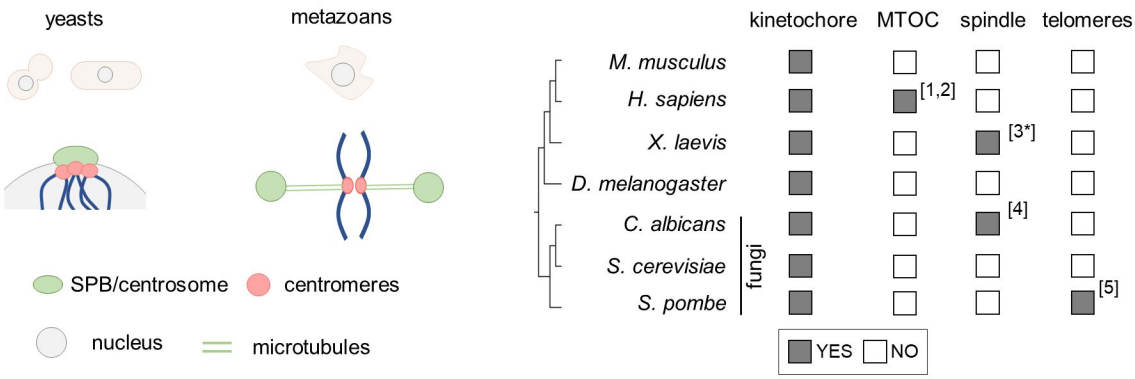
Supplementary Figure 7. *Polisetty et. al*